PROCEEDINGS BOOK

5th International Conference on New Trends in Chemistry

ICNTC CONFERENCE

INTERNATIONAL CONFERENCE ON NEW TRENDS IN CHEMISTRY

APRIL 22-24 2019
Athens/Greece
http://www.icntcconference.com/

ISBN: 978-605-67476-4-9

ICNTC'2019

5th International Conference on New Trends in Chemistry
Athens/Greece

Published by the ICNTC Secretariat

Editors:
Assoc. Prof. Dr. Dolunay Sakar Dasdan

ICNTC Secretariat
Büyükdere Cad. Ecza sok. Pol Center 4/1 Levent-İstanbul
E-mail: icntcconference@gmail.com
http://www.icntcconference.com

Conference organised in collaboration with Monre Tourism and Organization

SCINTIFIC COMMITTEE

Prof. Dr Josef Trna,
Masaryk Univerzoty – Czech Republic

Prof.Dr.Frieder W. Scheller,
Institute of Biochemistry and Biology, University of Potsdam, Potsdam, Germany

Assoc. Prof. Dr. Dolunay Sakar Dasdan,
Yıldız Technical University – Turkey
Conference Chair

PhD Dr. Habil. Agnieszka Kaczor,
Medical University of Lublin, Department of Medical Analytics,
Faculty of Pharmacy, Poland

PhD Dr. Habil. Agata Bartyzel,
University of Maria Curie-Sklodowska,
Faculty of Chemistry, Poland

PhD Dr. Habil. Daniel Ayuk Mbi Egbe,
Linz Institute for Organic Solar Cells, Linz,
Austria

Dr. Decha Dechechtrirat,
Department of Materials Science,
Faculty of Science, Kasetsart University, Thailand

Dr. Eduardo V. Ludeña,
Escuela Superior Politecnica del Litoral Ecuador
Center of Nanotechnology Research and Development (CIDNA), Guayaquil, Ecuador

Dr. Hatem M.A. Amin
Department of Chemistry
University of Oxford, UK

Dr. Mauricio Heriberto Cornejo Martinez,
Escuela Superior Politecnica del Litoral Ecuador
Center of Nanotechnology Research and Development (CIDNA), Guayaquil, Ecuador

CONFERENCE CHAIR

Assoc. Prof. Dr. Dolunay Sakar Dasdan
Yıldız Technical University – Turkey
Chemistry Department

ORGANIZATION COMMITTEE

Assoc. Prof. Dr. Dolunay Sakar Dasdan
Yıldız Technical University – Turkey

Assoc. Prof. Dr. Yelda Yalcin Gurkan
Namik Kemal University – Turkey
Chemistry Department

Dear Colleagues,

I am honoured to invite and send you this call for papers on behalf of Conference Organisation Board of "***5th International Conference on New Trends in Chemistry***", to be held at Athens, Greece dates between April, 22 – 24 2019

Limited number of Papers and Posters with the below mentioned topics will be accepted for our conference:

- Polymer Chemistry and Applications
- Pharmaceutical Chemsitry
- Computational Chemistry
- Bio Chemistry
- Physical Chemistry
- Analytical Chemistry
- Inorganic Chemistry
- Organic Chemistry
- Material Chemistry
- Environmental Chemistry

The most distinctive feature of ICNTC Conferences from other conference organizations is that the academicians working interdisciplinary can also attend to presentations performed in different speciality fields and they will also have the opportunity to meet with other academicians coming from various parts of the world.

- Selected Papers presented as Oral Presentation will be published as Special Issue Edition of **Journal of Indian Chemical Society. Journal of Indian Chemical Society** is indexed by Science Citation Index Expanded (SCI-E). (00194522)

Web site of journal : http://www. http://indianchemicalsociety.com/journal/index /

- Selected papers (limited as 5) presented as poster and oral related with material science consisting of microelectronics, photonics and micromachining will be published in **Material Science-Poland** after Material Science-Poland publication reviewing process. **Material Science-Poland is Science Citation Index Expanded Journal (ISSN 2083-1331)**

Web site of journal : http://www.materialsscience.pwr.wroc.pl

We kindly wait for your attendance to our congress to be held on 22 –24th of April 2019, with a hope to realize a satisfactory conference with it's social activities as well as the scientific ones and leaving a trace on your memories.

Respectfully Yours,
On Behalf of the Organization Committee of ICNTC Conference
Assoc. Prof. Dr. Dolunay SAKAR DASDAN
5th ICNTC 2019 | Conference Chair
Yıldız Technical University – Istanbul / Turkey
Chemistry Department

This Conference is organized in cooperation with **Smolny Institute of the Russian Academy of Education, St. Petersburg**

22 APRIL 2019 MONDAY

08:30-17:00 **: REGISTRATION**

MAIN HALL **: OPENING CEREMONY**

09:30 – 09:40
Welcome Speech **: Assoc. Prof. Dr. Dolunay SAKAR DASDAN / Yildiz Technical University**
Conference Chair

09:40 – 10:30
KEYNOTE SPEAKER **:Prof.Dr.Sotiris HADJIKAKOU**
Speech Title **: Conjugates of Non Steroidal Anti-inflammatory Drugs or Antibiotics, with metal ions (CoMeD's) towards the discovery and development of new therapeutic agents.**

10:30 – 10:40	**C O F F E E / T E A B R E AK**

HALL 1 / SESSION A (ACID)

SESSION CHAIR	**Prof.Dr. Sotiris HADJIKAKOU**	
TIME	**PAPER TITLE**	**PRESENTER** / CO AUTHOR
10:40 – 11:00	CO-Releasing Properties and Local Reactivity Descriptors of New $Re(CO)_3$(benzylbenzimidazole)(bpy)]OTf	**Elvan USTUN**
11:00 – 11:20	Production and *In Vitro* Characterization of Variously Doped and Formed S53p4 Bioactive Glass	**Efsun SENTURK**, Cem Batuhan CEVLIK, Ali Can OZARSLAN, Burcu KARAKUZU IKIZLER, Yeliz BASARAN ELALMIS, Sevil YUCEL
11:20 – 11:40	Binary Biomaterials (Inorganic material / Natural resin): Synthesis, Characterization and Performance for Adsorption of Dyes	**Sedef SISMANOGLU**, Hakan DURAN, Tuba SISMANOGLU
11:40 – 12:00	Effects of The Some Parameters on The Astaxanthin Productivity From *Haematococcus Pluvialis* Algae	Muharrem BOGOCLU, **Ceren KECECILER**, Cem ÖZEL, Bilge Sema TEKEREK, Sevil YÜCEL
12:00 – 12:20	Effects of Flue Gas As a CO_2 Source on The Cultivation of *Chlorella Protothecoides*	**Cem ÖZEL**, Muharrem Erdem BOĞOÇLU, Ceren KEÇECİLER, Ecem KAPLAN, Sevil YÜCEL
12:20 – 12:40	Thermoelectric Properties Of Poly (3,4-Ethylene Dioxythiophene)/Titanium Disulphide Composite	Naseer Subhi AHMED, **Ferdane KARAMAN**

12:40 – 13:40	**LUNCH**

HALL 1 / SESSION B (BLOOMING)

SESSION CHAIR	**Prof.Dr.Sevil Yücel**	
TIME	**PAPER TITLE**	**PRESENTER** / CO AUTHOR
13:40 – 14:00	Influences of Some 2-Aminothiazole Derivatives on Glutathione Reductase Activity	**Hasan KARADAG**, Emine EROGLU, Cumhur KIRILMIS
14:00 – 14:20	Preparation and characterization of bismuth oxychloride nanoparticles for the development of Photocatalytic performance	Bilal İbrahim DAN-IYA, **G. Selda POZAN SOYLU**
14:20 – 14:40	The Influence of Chemical Composition on Peroxidation Kinetics of Palm and Nut Oils	**Temel Kan BAKIR**
14:40 - 15:00	Kinetics and mechanism of pyridine substitution of $[(\eta^3\text{-}C_3H_5)Mo(CO)_2(X)(py)_2]$ (X = Cl, Br; py = pyridine) by1,10-phenanthroline	**Khalil J. ASALI**

15:00 – 15:20	**C O F F E E / T E A B R E AK**

HALL 1 / SESSION C (CATALYSIS)

SESSION CHAIR	**Dr.Esin BOZKURT KOPUZ**	
TIME	**PAPER TITLE**	**PRESENTER** / CO AUTHOR
15:20 – 15:40	Steric and Electronic Requirements for Atropisomerization in Heterocyclic Analogues of Biaryls	**Ilknur DOGAN**
15:40 – 16:00	Investigation of changes in antioxidant activity of some *Pleurotus* species by using composts including different metal salts	**Mertcan KARADENIZ**, Temelkan BAKIR, Sabri UNAL
16:00 – 16:20	Single Enantiomer Thioureas As Chiral Solvating Agents	**Sule EROL GUNAL**
16:20 – 16:40	Non Linear Phenomena in Cellular Automata Simulations of Metal Corrosion and Passivity	Jan STĘPIEŃ, **Janusz STAFIEJ**
16:40 – 17:00	Investigation of Sensitivity Precision of Smaller Particles Through The Asymmetric Nanopo	**Dürdane YILMAZ**, Dila Kaya, Kaan Kececi, Ali DİNLER
17:00 – 17:20	Fabrication, Modification and Sensing Behaviour of Quartz Micro/ Nanopipettes	**Dila KAYA**, Kaan KECECI, Durdane YILMAZ
17:20 - 17:40	Discrete-Time Controllers For Temperature Control of A Polystyrene Polymerization Reactor	**Semin ALTUNTAŞ**, Hale HAPOĞLU, Gülay ÖZKAN
18:00 – 18:20	Varying the Granulometric Composition of an Electromelted Corundum Based Ceramic with A Porcelain Binder To Control Its Open Porosity and Strength	**Zaw Ye Maw Oo**

23 APRIL 2019 TUESDAY

08:30-17:00 : REGISTRATION

HALL 1 / SESSION D (DILUENT)

SESSION CHAIR	**Assoc.Prof.Dr.Emel AKYOL**	
TIME	**PAPER TITLE**	**PRESENTER** / CO AUTHOR
09:00 – 09:20	Nanoencapsulation of polar bioactive compound	**Flavio MASSIGNAN**, Éva KISS
09:20 – 09:40	Removal of Bentazon and Metalaxyl Pesticides From Aqueous Solutions By Almond and Chestnut Shells: Optimization, Kinetics and Isotherm Studies	Barış DİLER, **Dilek KILIÇ APAR**
09:40 – 10:00	Absorbtion of Glyphosate-Ipa Herbicide on Mesoporous Silica Nanoparticules	**Birsen Sengul OKSAL,** Yunus SENTURK
10:00 – 10:20	Degradation Mechanism of Capsaicin Molecule in gaseous phase: Moleculer Modeling and DFT study	**Bahar EREN,** Yelda YALCIN GURKAN, and Yasemin IYIDOGAN
10:20 - 10:40	Structural and electronic properties of layered semiconductor chalcogenide crystals: $TlGaSe_2$, $TlGaS_2$, and $TlInS_2$	**Burak GURKAN,** Savas BERBER
10:40 – 11:00	Water Quality In Istanbul, Marmara Sea	**Esin BOZKURT KOPUZ**, Gökberk KARA, Burak DİNÇER, Yeşim GÜRTUĞ

11:00 – 11:20	**C O F F E E / T E A B R E AK**

HALL 1 / SESSION E (ELECTRON)

SESSION CHAIR	**Assoc.Prof.Dr.Nuriye AKBAY**	
TIME	**PAPER TITLE**	**PRESENTER** / CO AUTHOR
11:20 – 11:40	Interaction of Insoluble Silica Gel Derivatives With Signaling Nucleotide of Bacteria	Secil TURKSOY, Merve BICER, **Gokce MEREY**
11:40 – 12:00	The Treatment of Detergent Industry Wastewaters By Supercritical Water Oxidation	**Ekin KIPÇAK**, Sema ŞENTÜRK, Mesut AKGÜN
12:00 – 12:20	In Situ Synthesis Of Triglyceride Oil Based Polymer Clay Nanocomposite	A. Tuncer ERCIYES, Yagmur BAYRAM, **Emel AKYOL**
12:20 – 12:40	Biosorption of Remazol Orange Rgb By Kefir Biomass Under Sonication	**Hatice MUTLU**, Dilek KILIÇ APAR
12:40 – 13:00	Ag Particles Deposition on Polyacrylonitrile Fibers Grafted By Acrylamide, Acrylamide-Itaconic Acid and Acrylamide-Maleic Acid	Zeynep OKAY, **Meryem KALKAN ERDOĞAN**, Meral KARAKIŞLA and Mehmet SAÇAK

13:00 – 14:00	**LUNCH**

HALL 1 / SESSION F (FUNCTION)

SESSION CHAIR	Dr.Flavio MASSIGNAN	
TIME	**PAPER TITLE**	**PRESENTER** / CO AUTHOR
14:00 – 14:20	Preparation of A Novel Gold Nanocluster-Based Biosensor Using Egg White Protein and Its Application for Measuring Prooxidant Activity	**Esin AKYÜZ**, Furkan Burak ŞEN, Mustafa BENER, Kevser Sözgen BAŞKAN, Esma TÜTEM, Reşat APAK
14:20 – 14:40	Temperature Controled Infrared Drying Kinetics of Mussels	Sema SEVIM, Emek DERUN, Nurcan TUGRUL, Ibrahim DOYMAZ, **Azmi Seyhun KIPCAK**
14:40 – 15:00	A highly selective non-enzymatic H_2O_2 sensor supported on Eupergit CM decorated with PdMoAg nanoparticles	**Hilal ÇELİK KAZICI**, Fırat SALMAN, Mehmet Sait İZGİ, Ömer ŞAHİN
15:00 – 15:20	Development of Chitosan-Based Edible Biocomposite Films Incorporated with Kumquat Peels Extract as Food Packaging	Fatmagül ŞAHIN, **İlknur KÜÇÜK** and İbrahim DOYMAZ
15:20 – 15:40	A Theoretical Study of The Reaction of Dimethyl Phosphoramidate With Hydroxyl Radicals	**Seyda AYDOGDU**, Arzu HATIPOGLU
15:40 – 16:00	Increased Solubility And Efficacy of Water Insoluble Flavonoids With N,N-Dimethylalkyl Groups Carrying Calix[N]Arenes	**Serdar KARAKURT**, Mehmet OGUZ, Mustafa YILMAZ

16:00 – 16:20	**C O F F E E / T E A B R E AK**

HALL 1 / SESSION G (GRAVITY)

SESSION CHAIR	Prof.Dr.Khalil J. ASALI	
TIME	**PAPER TITLE**	**PRESENTER** / CO AUTHOR
16:20 – 16:40	New method for the synthesis of the 1,5-methanoazocino[4,3-*b*]indole by intramolecular cyclization of -1,2,3,4-tetrahydrocarbazoles mediated by tetrachloro-1,4-benzoquinone	**Nesimi ULUDAG**, Naki ÇOLAK
16:40 – 17:00	Silver Nanoparticles as a scavenging material for new assay for polyphenols metal scavenging activity	**Abdelaziz ELGAMOUZ**, Alaa Alsaidi, Rana Alsaidi, Chahlaa Naser Nassab
17:00 – 17:20	Structure/Reactivity Properties of Manganese-Based Imidazole Complexes: A DFT Study	Gaye GÜNGÖR**, Dolunay ŞAKAR DAŞDAN,** Elvan ÜSTÜN
17:20 – 17:40	Novel carbon quantum dots and their bioimaging applications	**Fatima OUANZI** , Imre BERTÓTI, Miklós MOHAI, Tamás KOLONITS, Kata HORVÁTI, Szilvia BŐSZE, Gergő GYULAI

HALL 1 / POSTER SESSION H

SESSION CHAIRS	ASSOC.PROF..DR.DİLEK KILIÇ APAR ASSIST.DR.ILKNUR KUCUK Janusz STAFIEJ Abdelaziz ELGAMOUZ Fatima OUANZI	
18:00 – 19:00	**PAPER TITLE**	**PRESENTER /** CO AUTHOR
An Investigation Of Stability And Activity Of Poly(Methyl Vinyl Ether-Alt-Maleic Anhydride) Copolymer In The Different Phs And Simulated Body Fluids		Ata AKSOY, İmren ÇOTUK ULUSOY, Kadir ÇAKIRAL, **Dolunay ŞAKAR DAŞDAN**
Effect Of Dopant Localization İn The Micelles On The Formation Of Uniaxial And Biaxial Lyotropic Cholesteric Phases		**Esra SAHIN**, Baris OKUYAN, Erol AKPINAR
Development And Optimization Of An Hplc Method For The Simultaneous Analysis Of A Multi Component Drug Product By The Help Of Central Composite Design		Şule DİNÇ-ZOR, **Evridiki PİNGO,** Özlem AKSU DÖNMEZ, Bürge AŞÇI
Modeling Particle Size of Polyacrylic Acid-Copper(Ii)-Bovine Serum Albumin Ternary Complex In Salt Solution		Dolunay ŞAKAR DAŞDAN, MESUT KARAHAN, **FATMA NOYAN TEKELİ**, GÜLHAYAT GÖLBAŞI ŞİMŞEK
Synthesis and Thermoelectric Properties of Polythiophene/Poly(3,4-ethylene dioxythiophene) Nanocomposites under Magnetic Field		Keziban HUNER, **Ferdane KARAMAN**
Influence of Some Parameters on The Protective Power of Caffein Against Copper Corrosion		**Hiba MESSAOUDI**, Mohamed LITIM, Maamar SLIMANE, Djilali BEKHITI
Adsorption Behavior And Surfaca Analysis Of Caffeine As A Green Corrosion Inhibitor For Copper		**Hiba MESSAOUDI**, Bahadir KESKİN
Catalytic hydrodeoxygenation of bio-oil in a fixed bed reactor		WANG JUNDONG, NOURELHOUDA BOUKAOUS, **LOKMANE ABDELOUAHED** , CHETNA MOHABEER, LIONEL ESTEL, BECHARA TAOUK
Detailed modelling of Anaerobic digestion with experimental validation		**LOKMANE ABDELOUAHED**, ANDRES MARTINEZ, BECHARA TAOUK, LIONEL ESTEL
Improving of Dye Uptake and Moisture Absorption Abilities of Polyacrylonitrile Fiber By Grafting of Hydroxymethyl Methacrylate		Merve BARUT, **Meral KARAKIŞLA** and Mehmet SAÇAK
Lyotropic Uniaxial and Biaxial Cholesteric Phase Properties of Potassium Alkanoate/Decanol/H_2O/Brucine Sulfate Mixtures		**Nazli UYGUR**, Seda UYANIK, Erol AKPINAR
Functionalized Clinoptilolite For Removal of Soluble Dyes in Aqueous Solution		**Neli MINTCHEVA**, Gospodinka GICHEVA, Lyubomir DJERAHOV, Marinela PANAYOTOVA
Preparation Of Silver Nanoparticles-Zeolite Nanocomposite And Its Potential Application As An Antibacterial Agent In Water Treatment		**Neli MINTCHEVA,** Gospodinka GICHEVA, Marinela

	PANAYOTOVA, Lyubomir DJERAHOV
Naproxen Derivative Interaction Properties With CT-DNA	**Nuriye AKBAY**, Zeynep KOKSAL, Tugba TASKIN-TOK, Ayse UZGOREN-BARAN
Stimuli-responsive polyzwitterionic microgels with tunable UCST – LCST and study of their anti-polyelectrolyte effect in salt solutions	**Pabitra SAHA**, Nikhil K. SINGHA, Andrij PICH
Micellization properties of some tetradecylalkylammonium bromide surfactants	**Sezin CETINKAYA**, Emre GUNER, Erol AKPINAR
Evaluation of extraction and HPLC separation of polyphenol compounds in *Mallotus oppositifolius* (Geisel) Müll. Arg.	**Soleya DAGNON**, Nikoleta MARGOVA, Dimitar BOJILOV, Kouadio KOUASSI
UHPLC-MS investigation of polyphenol composition in *Clinopodium vulgare*	Dimitar BOJILOV, **Soleya DAGNON**, M. KIRILOVA
Hydroxyl Radical Decomposition Reaction of Ciclacillin Molecule	**Yelda YALCIN GURKAN**, Nilay SAKARYA, Bahar EREN

24 APRIL 2019 WEDNESDAY

12:00 – 18:00	**SOCIAL PROGRAM FOR CONFERENCE PARTICIPANTS**

5th International Conference on New Trends in Chemistry

A highly selective non-enzymatic H_2O_2 sensor supported on Eupergit CM decorated with PdMoAg nanoparticles

Hilal ÇELİK KAZICI[1], Fırat SALMAN[2], Mehmet Sait İZGİ[3], Ömer ŞAHİN[3]

[1,2] Van Yüzüncü Yıl University, Faculty of Engineering, Department of Chemical Engineering, Van, Turkey

e-mail: hcelik@eng.ankara.edu.tr, hilalkazici@yyu.edu.tr

e-mail: frtsalman.che@gmail.com

[3] Siirt University, Faculty of Engineering, Department of Chemical Engineering, Siirt, Turkey

e-mail:saitizgi@gmail.com

Abstract

At present, Pd, Mo and Ag multimetallic nanoparticles were synthesized by the chemical reduction method based on the dissolution of metal salts and the reduction of these metal salts to zero valence. Novel Eupergit CM supported Pd, Mo, and Ag multimetallic nanoparticles were characterized with X-ray Diffraction (XRD), Energy Dispersive X-ray Spectroscopy (EDS) and Scanning Electron Microscopy (SEM) techniques. The electrochemical behaviour of the modified electrode was investigated by Cyclic Voltammetry (CV) and Chronoamperometry (CA). The effect of third metal addition was examined through electrochemical Hydrogen peroxide (H_2O_2) sensing ability. The resulting sensor exhibits high sensitivity and good reproducibility. Several milk samples were analysed for their H_2O_2 contents using a PdMoAg/ Eupergit CM sensor system. The contents were determined using the standard addition method. As could be seen, there was a close relationship between the values found for the H_2O_2 measurements in the sensor and those real values on the sample. The resulting PdMoAg/ Eupergit CM nanocatalysts offer new features for electrochemical devices due to the synergistic effect of trimetallic nanoparticles.

Key Words: *Multimetallic, Hydrogen peroxide, Eupergit CM, Milk*

I. Introduction

Hydrogen peroxide (H_2O_2) has been extensively studied in quantitative analysis, clinical diagnosis, chemical, biological, food and pharmacy [1,2]. H_2O_2 is a multifunctional oxidizing agent because it is not only an important intermediate of enzymes that catalyze biological reactions, but is also used in wastewater treatment and the textile industry [3]. In addition, this well-known type of reactive oxygen is considered dangerous because it can lead to brain damage. As a result, it is important and worrying for H_2O_2 to develop a reliable, simple, fast and precise analytical method for them. A number of analytical techniques such as titrimetry, spectrophotometry,chemiluminescence and electrochemistry [4,6] have been applied for this purpose. Amongst these, the application of electrochemical methods are the most promise assay due to its high specificity, sensitivity, accuracy, rapidness, requirement for low volumeof analyte and simplicity [7,8].

The important experimental parameters such as concentration, scan rate, electroactive surface area and real sample were investigated to establish an optimized sensor. The analytical

performance of the sensor was assessed with the optimized parameters using the chronoamperometry for the quantification of H_2O_2. Finally, the reproducibility was verified.

2. Experimental section

2.1. Reagents and materials

H_2O_2, sodium dihydrogen phosphate (NaH_2PO_4), disodium hydrogen phosphate (Na_2HPO_4) and sodium borohydride ($NaBH_4$, 97% purity) were purchased from Sigma-Aldrich. All solutions were prepared and diluted with ultrapure water (Millipore Milli Q system, 18.2 MΩ).

2.2. Synthesis of the PdMoAg/ Eupergit CM and Preparation of the PdMoAg/ Eupergit CM/NGCE electrode sensor

The specified amounts of Pd, Mo and Ag were weighed and dissolved in pure water. Subsequently, the prepared solution was added into Eupergit CM. The final solution was stirred at room temperature for 12 h until the volume reduced around 4 mL. Consequently, 50 mL $NaBH_4$ aqueous solution was introduced to the prepared solution as dropwise into under continuous stirring at 5 ^oC. The obtained black pellet was then collected and washed with distilled water and ethanol, respectively. The final product was dried at 80 ^oC for 5 hour under N_2 gas. The synthesized PdMoAg/ Eupergit CM supported catalyst was used to measure hydrogen generation rate versus time using water displacement method.
Before modification, GCE working electrode was polished with 0.3 μm alumina powder and sonicated for at least 10 min in distilled water. Then, the electrode was rinsed alternatively with methanol and water and dried under a nitrogen stream. Electrochemical experiments were performed using a Biologic SP50 potentiostat controlled by a PC in a conventional three electrode glass cell. The working electrode was a (GCE) a (diameter=3 mm, electrode surface area=0.071 cm^2) modified with catalyst sample. Pt wire and Ag/AgCl (3 M KCl) electrode were employed as counter and reference, respectively.

3. Results and discussion

The powder XRD analysis was employed to confirm the crystallinity of the PdMoAg catalyst. the XRD patterns of the catalyst demonstrated four main reflections at 38.13^0 (111) 44.24^0 (200), 65.27^0 (220) and 77.63^0 (311) as indicated in figure 1. These diffraction peaks are the characteristic reflection of face-centered cubic (fcc) structure of pd. (jcpds: 87-0641) the diffraction pattern at 38.13^0 (111) has more intensity than other diffraction patterns. This situation indicates the preferred direction for the growth of the pdmoag catalyst. There are no characteristic peaks of metal mo and ag detected in the xrd pattern. It is reasonable that the mo and ag content is extremely low in the PdMoAg catalyst. Based on the half width of the most intense reflection 38.13^0 (111), the average crystallite size of the pdmoag catalyst was calculated as approximately 4 nm using the scherer equation.

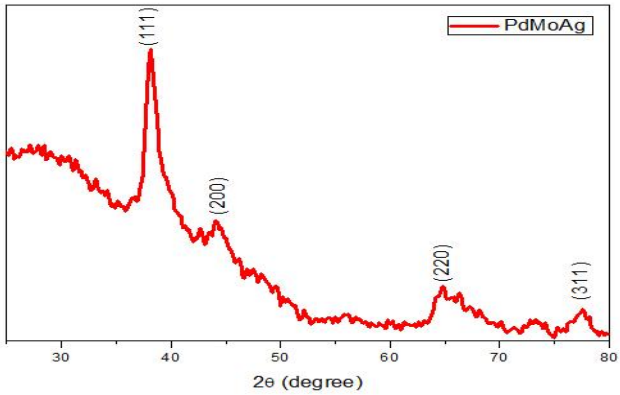

Fig. 1. The XRD patterns of PdMoAg catalyst

SEM images and EDS mapping of PdMoAg/ Eupergit CM are given in Figure 2. It is clear that Pd, Ag and Mo is distributed homogenously on the Eupergit CM support. Furthermore, the Pd, Mo and Ag atomic ratio is close to the nominal values.

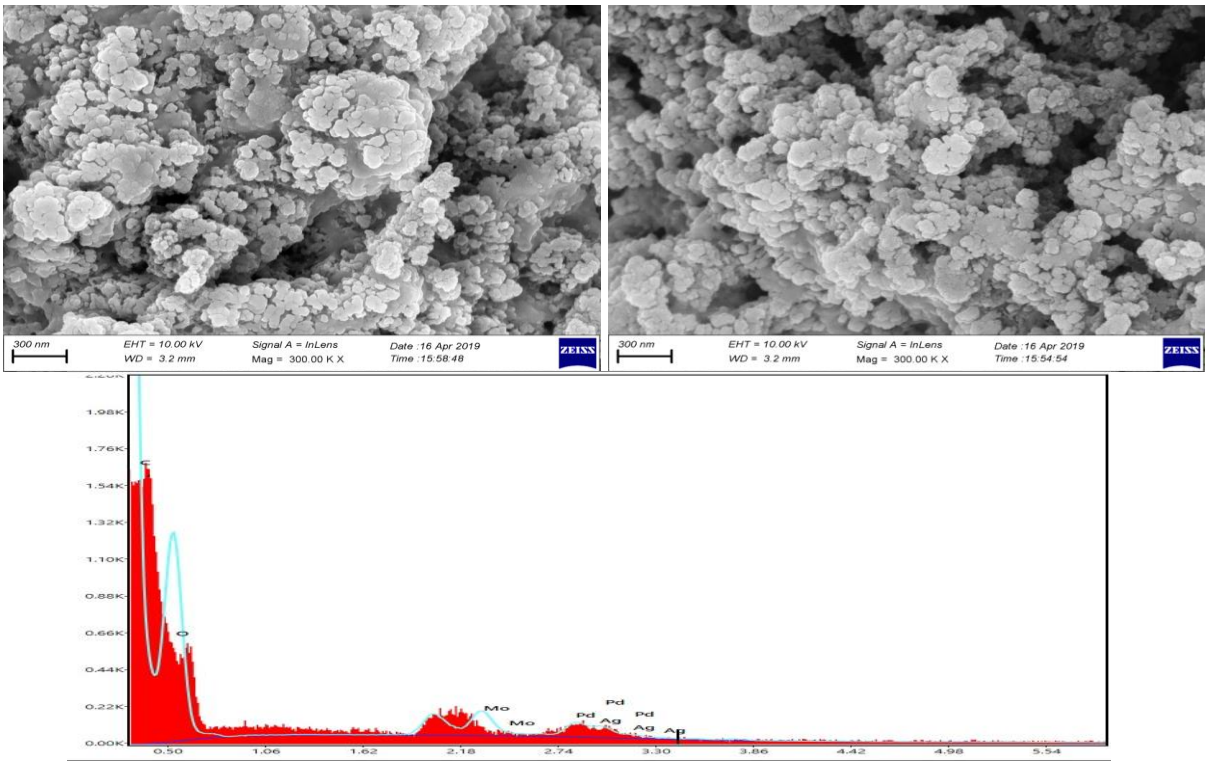

Fig.2. SEM images and EDS mapping PdMoAg/ Eupergit CM

Electrochemical measurements of H_2O_2; the effect of concentration of H_2O_2 using PdMoAg/EupergitCM/NGCE

The effect of H_2O_2 concentration on the H_2O_2 electrocatalytic activity of PdMoAg/EupergitCM/NGCE was conducted at different H_2O_2 concentrations (0 -25 mM) in 0.1 M PBS by CV.

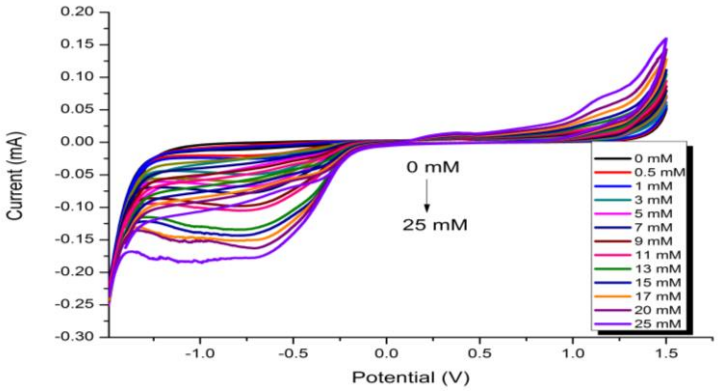

Fig. 3. The effect of concentration of H_2O_2 on cathodic and anodic peak current in PBS (pH 7) 50 mVs^{-1}

Also, the reduction current is linearly increased with increasing H_2O_2 concentration and broad peaks were obtained at higher H_2O_2 concentrations. The sensor exhibited a very linear behavior in the range of 0-25 mM, after which the surface active sites were saturated.

The Effect of Scan Rate

The scan rate was measured in response to the electrochemical reaction of 5 mM H_2O_2 in 0.1 M PBS (pH 7) (Fig. 4). Figure 4 shows a linear relationship between the cathodic peak current and the scan rate versus the square root, which is a typical diffusion-controlled reaction of H_2O_2 for the PdMoAg/EupergitCM/NGCE electrode and the equation could be expressed as;

$$I_{cathodic}\ (\mu A) = -0.0059\upsilon^{1/2} - 0.0079\ (R^2 = 0.9833)$$

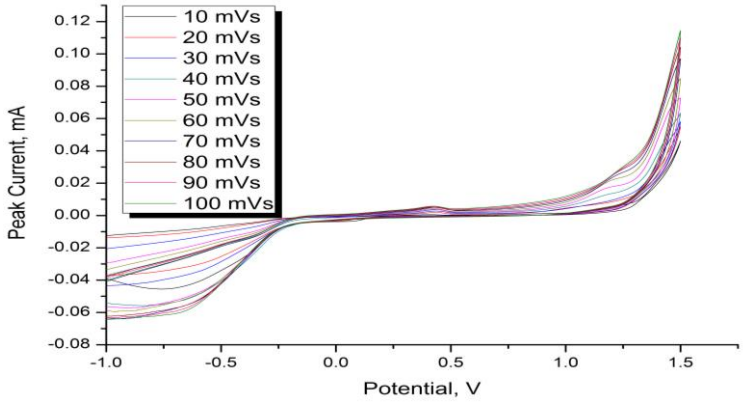

Fig. 4. a) PdMoAg/EupergitCM/NGCE different Scan rate: 10-30-50-70-90-100 mV s-1 in 5 mM H_2O_2 in Ar-saturated 0.1 M phosphate buffer (pH 7.5) solution **b)** The plot of the peak current (Ip) against the square root scan rates (v)

The electroactive surface area ESA of the PdMoAg/EupergitCM/NGCE electrodes

The ESA of the PdMoAg/EupergitCM/NGCE electrode was calculated according to the slope of the Ip vs.$v^{1/2}$ plot for a known concentration of $K_2Fe(CN)_6$, based on the Randles–Sevcik equation:

$$Ip = 2.69 \times 10^5\ A \times D^{1/2}\ n^{3/2}\ \vartheta^{1/2}\ C \qquad (1)$$

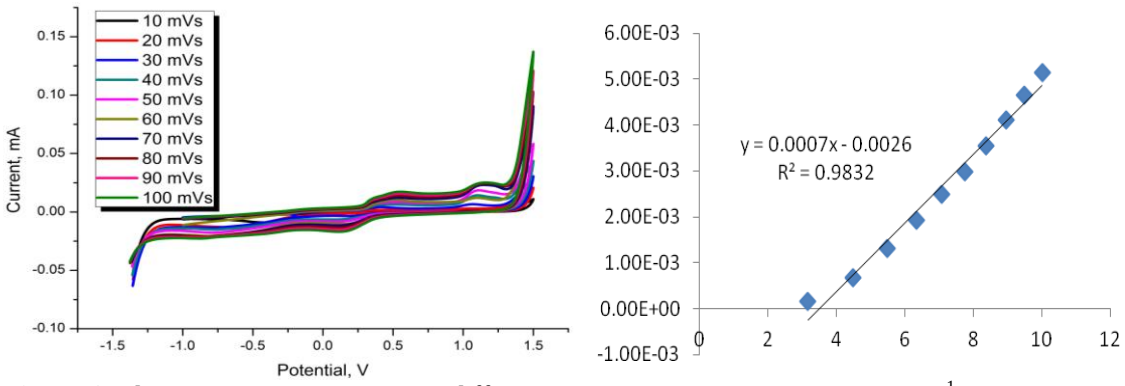

Fig. 5. a) PdMoAag/EupergitCM/NGCE different scan rate: 10-30-50-70-90-100 mv s^{-1} in 0.05 mm $K_2Fe(CN)_6$ solution **b)** the plot of the peak current (ip) against the square root scan rates $(v)^{1/2}$

From the slope of the $Ip–v^{1/2}$ relation, the microscopic area was calculated 0.2 cm^2.

Repeatability of sensor

Typically, more than one measurement of a homogeneous sample by the same analyst occurs, for example, as an analysis of the same four samples. The repeatability of the microporous microstructure pre-alloyed PdMoAag/EupergitCM/NGCE was analyzed using 5 mM H_2O_2 (Fig. 6).

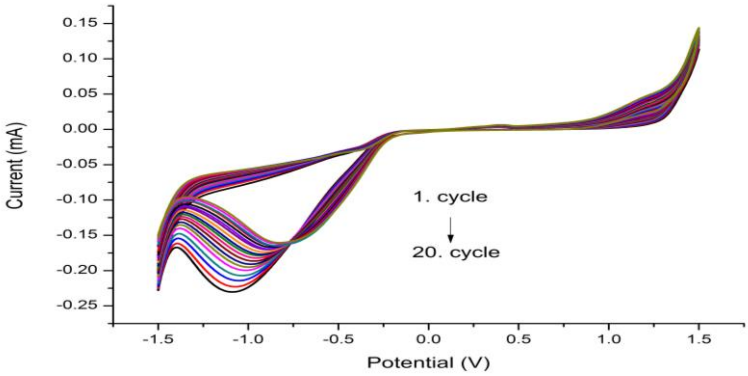

Fig. 6. Repeatability of sensor

CA (Chronoamperometry) Measurements

Fig. 7 displays the typical amperometric i–t curve of H_2O_2 redox reaction at PdMoAag/EupergitCM/NGCE electrode after the successive addition of H_2O_2.

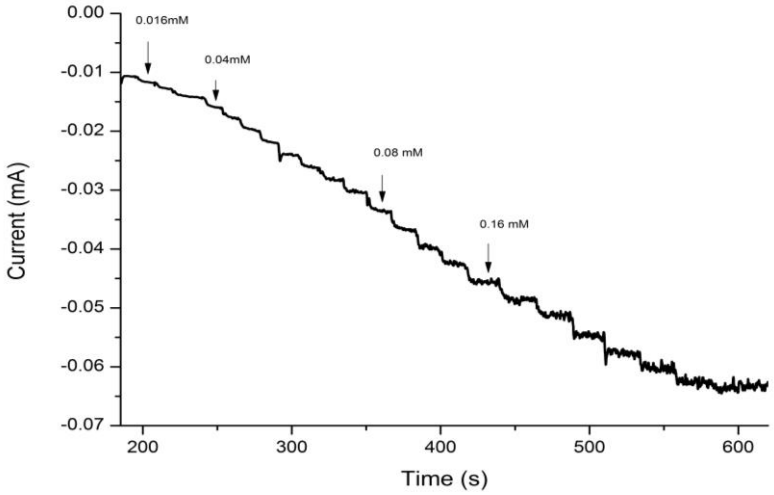

Fig. 7. Dependence of the CA diagrams with H_2O2 concentration in PBS buffer, pH 7, ϑ=50 mVs^{-1}

The detection limit was calculated to be 0.010 mM based on the signal-to-noise ratio of 3 [9].

Real samples

The practical feasibility of H_2O_2 detection in the real sample was evaluated in milk solution. Before measurements, the real sample was diluted 100 times with PBS (Fig. 8). The results indicate that PdMoAag/EupergitCM/NGCE can be applied for the detection of H_2O_2 in real samples.

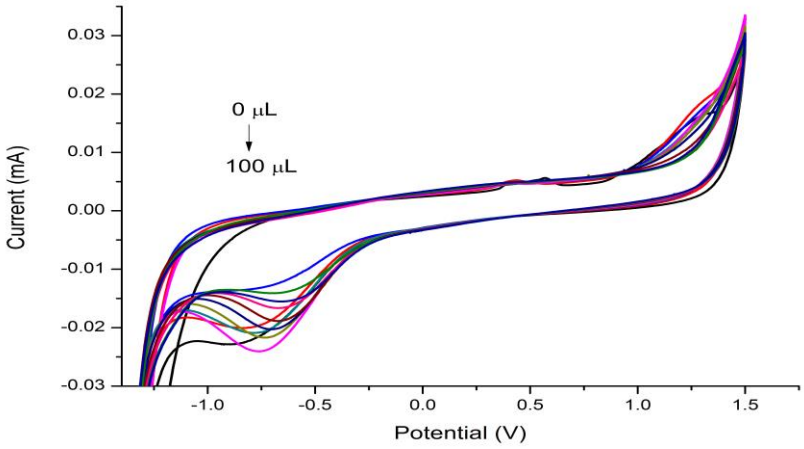

Fig. 8. Determination of H_2O_2 in milk solutions

Conclusion

In conclusion, we have successfully synthesized PdMoAag/EupergitCM/NGCE with chemical reduction method. So, as a result, this H_2O_2 sensor exhibits an good performance in detecting H_2O_2, including high sensitivity, low detection limit, good reproducibility. Thus, it might be an attractive electrode for non-enzymatic H_2O_2 detection and other electrochemical applications.

References

[1] Wang YH, Yang XJ, Bai J, Jiang X, Fan GY (2013) Biosensors & Bioelectronics, 43:180-185.
[2] Piwkowska A, Rogacka D, Jankowski M, Kocbuch K, Angielski S (2012) J. Cell. Physiol. 227:1004–1016.
[3] Butwong N, Zhou L, Ng-eontae W, Burakham R, Moore E, Srijaranai S, Luong JHT, Glennon JD (2014) J. Electroanal. Chem. 717–718: 41–46.
[4] Pinkernell U, Effkemann S, Karst U (1997) Anal. Chem. 69:3623–3627
[5] Tahirovic A, Copra A, Omanovic-Miklicanin E, Kalcher K (2007) Talanta 72:1378–1385
[6] Peng Y, Jiang DL, Su L, Zhang L, Yan M, Du JJ, Lu YF, Liu YN, Zhou FM (2009)
Anal. Chem. 81:9985–9992.
[7] Afraz A, Rafati AA, Hajian A (2013) J Solid State Electrochem. 17:2017–2025.
[8] Zhan K, Liu H, Zhang H, Chen Y, Ni H, Wu M, Sun D, Chen Y J (2014). Electroanal. Chem. 724:80–86.
[9] Kazici HC, Salman F, Caglar A, Kivrak H, Aktas N (2018) Fullerenes, Nanotubes and Carbon Nanostructures 26 (3); 145-151

Degradation Mechanism of Capsaicin Molecule in gaseous phase: Moleculer Modeling and DFT study

Bahar EREN[1], Yelda YALCIN GURKAN[2], and Yasemin IYIDOGAN[2]

[1] Tekirdag Namık Kemal University, Faculty of Agriculture, Tekirdag, Turkey, beren@nku.edu.tr

[2] Tekirdag Namık Kemal University, Department of Chemistry, Tekirdag, Turkey, yyalcin@nku.edu.tr

Abstract

Capsaicin is known as a considerably strong and stable alkaloid, which is formed in nature only in hot pepper as crystal. Capsaicin is a kind of oil, which is the main component obtained from chilli paprika, and is also known as 'oleoresin capsicum'. In addition to its pharmacological use, it is also widely used as a pepper spray, which is produced through dissolving the oil in organic solvents such as chloroform, alcohol and ether as 1-10% solution. The known harmful effects of this molecule can be exemplified as irritation and lacrimation in the eye, asthma, various respiratory irritations, and irritating effects on epithelial tissues, although the exposed area is washed up with water. In this study, in order to eliminate the harmful effects of capsaicin, the reaction of the fragmentation of capsaicin with OH radical was analysed. Quantum chemical calculations of Density Functional Theory (DFT) were used to analyse the structural and physical characteristics of capsaicin and its derivatives. The aim of this study is to estimate the degradation mechanism of capsaicin molecule in gaseous phase for each fragmentation and to compare the energy values and stabilities of this molecule and its five stable fragments in solvents, ethanol, diethyleter, and chloroform. Calculation of the probable reaction path of this molecule was made, and their most stable state in the thermodynamic frame was determined for these phases.

Key Words: *Capsaicin, Pepper Gas, Gaussian 09, DFT, OH radical*

1. Introduction

Capsaicin is a considerably strong and stable alkaloid, which is formed in nature only in hot pepper [1]. There are many studies revealing that capsaicin decreases the amount of lipid tissue as well as triglyceride levels of liver and serum triglyceride by increasing lipid peroxidation, and that in an in vitro environment, it plays an inhibiting role in glycogen metabolism in skeletal muscles. In addition, capsaicin is known to have various effects on body temperature, digestive system, and cardiovascular system [2]. In many conducted studies, it was stated that natural plants have significant effects on the treatment or prevention of numerous diseases. Red pepper, in addition to being a vegetable and medicinal plant, has also been used as flavouring or colouring natural source in foods for a long time. It is believed that red pepper (Capsicum annuum L.) has preventive or therapeutical characteristics against many diseases such as asthma, rheumatism, neuralgia, lumbago, or pharyngitis, and that it is also an appetizer [3]. Capsaicin is a kind of oil extracted from red peppers, namely Capsicum annum or Capsicum frutescens of Solanea genus, and is known as 'oleoresin capsicum' (OC). It is not soluble in water, but can be dissolved in organic solvents such as alcohol, ether, and chloroform.

In this study, by conducting conformation analysis of Capsaicin, hereinafter referred to as CA, the most appropriate conformers with the lowest energy and the most stable ones were determined. The geometric optimizations of the molecule and its molecular properties were determined at B3LYP/6-31G(d) level of DFT study [4]. As a result of the quantum chemical calculations, load densities, energy values, and geometric parameters for CA molecule and various fragments of this molecule were determined. The degradation mechanism of capsaicin molecule in gaseous phase for each fragmentation and to compare the energy values and stabilities of this molecule and its five stable fragments in solvents, ethanol, diethyleter, and chloroform were determined.

This study was conducted in order to find out whether this molecule, being named CA molecule in our study, would be fragmented in the nature under the formation of CO_2, H_2O and other small molecules. In this study, the kinetics of the degradation reaction path of CA molecule with OH radical was analysed theoretically through the density functional theory (DFT) method. Theoretical calculations were carried out at DFT/B3LYP/631G(d) level in gas-phase [4,5].

1. Methodology

In photocatalytic degradation reactions of CA molecule, it is possible that products more harmful than those in the original material could be formed. For this reason, it is crucial to apprehend the nature of the primary intermediate products before conducting a photocatalytic degradation reaction experimentally. Calculations carried out by quantum mechanical methods provide the most reliable and precise information. Hence, due to the yield produced being the same, photocatalytic degradation reactions of CA molecule and its hydroxyl derivatives were based on the direct reaction of these molecules with OH radical. With this aim, the kinetics of the reactions of CA molecule with OH radical was theoretically analysed. The study was initiated with O molecule and then exposed to reaction with OH radical and the reaction yields were modelled in gas-phase.

Experimental results in the scientific literature revealed that OH radical detaches a hydrogen atom from saturated hydrocarbons, and OH radical is added to unsaturated hydrocarbons and materials with this structure [6-8]. Therefore, possible reaction paths for the analysed reactions were calculated. In this study, primarily the conformation analyses of CA were conducted, and the conformers with the lowest energy, or in other words, the most stable ones were determined. Geometric optimizations of the molecule were carried out at DFT/ B3LYP/6-31G(d) level. As a result of the quantum chemical calculations, the geometric parameters, energy, enthalpy, and Gibbs-free energy, and also load density, and mulliken loads in gas-phase were determined [4,6].

In this study, Gaussian 09 packaged software was used. This electronic structure provides state-of-the –art capabilities for modelling. Gaussian 09 is a considerably comprehensive programme, which includes molecular mechanics, semi-empiric, and ab initio methods. The programme has a wide range of theory and basic set options for the three methods. With the Gaussian 09 programme, the energies of atoms and molecules can be calculated, geometric optimizatipons can be made, and energy dependent vibration frequencies, force constants, and dipole moments can be calculated. The programme can navigate potential energy surfaces and scan minima, transition states and reaction pathways. The programme can also test the stability of the molecular wave function.

The investigated reaction system was composed of OH radical, which are open-shell species. It is known that open-shell molecules cause severe problems in quantum mechanical calculations [9]. DFT methods, taking the electron correlation into account, use the precise electron density to calculate molecular properties and energies. The applicability of the method ranges from atoms, molecules and solids to nuclei and quantum and classical fluids. DFT predicts a great variety of molecular properties such as molecular structures, vibrational frequencies, atomization energies, ionization energies, electric and magnetic properties, reaction paths. Spin contamination does not affect them and hence, for calculations involving open-shell systems, they become favourable. DFT calculations were made by the hybrid B3LYP functional combining the HF and Becke exchange terms with the Lee–Yang–Parr correlation functional. In such calculations, it is the 6-31G(d) basis set that is used [4,6,9-11].

2. Findings

According to Fig. 1 of CA molecule and optimized figures of three stable fragments of CA molecule to Fig.2.

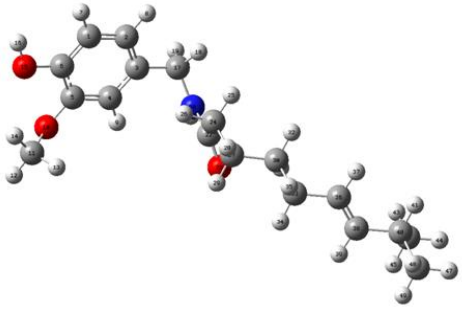

Fig. 1. Optimized state of the same CA molecule. (blue, nitrogen; white, hydrogen; red, oxygen; grey, carbon)

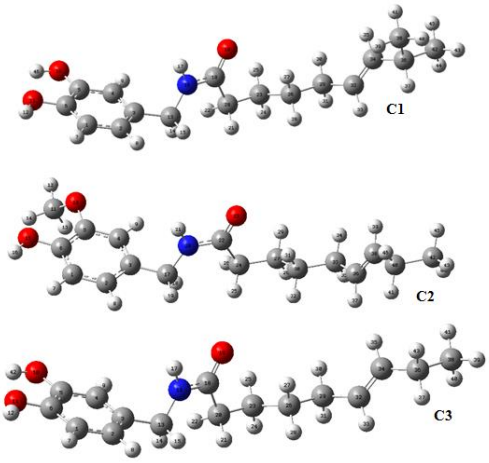

Fig. 2. Optimized figures of three stable fragments of CA molecule (C1, C2, C3; blue, nitrogen; white, hydrogen; red, oxygen; grey, carbon)

The probable stable fragmentation pathway of CA molecule is given in Fig. 3.

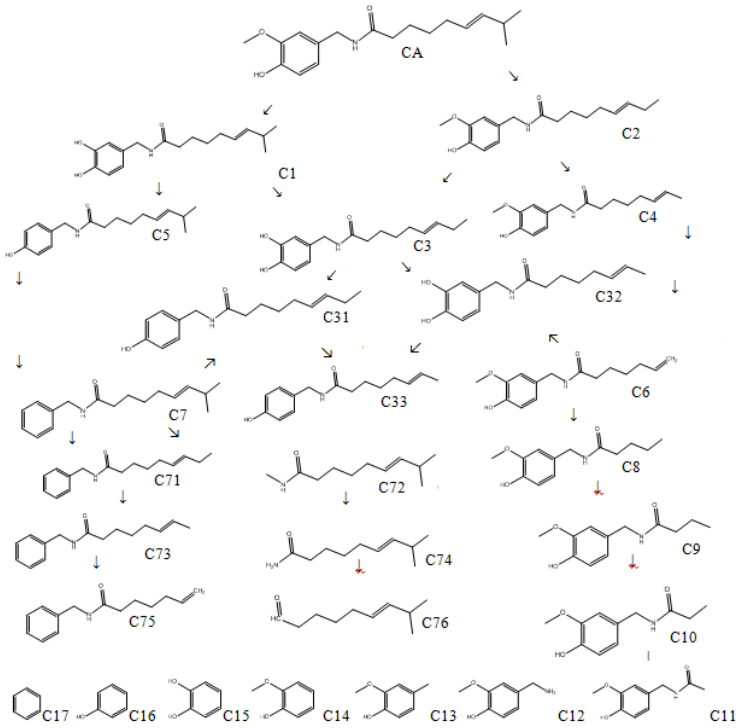

Fig. 3. Probable fragmentation paths of CA molecule

Energy values in gas phase of the CA molecule and its all stable fragments are given in this table. As seen in this table, all fragments have negative values. Reaction pathways from C1 to C5 are estimated through these energy values given in the Table 1.

Table1. Energy, enthalpy and Gibbs-free energy values (Au) of CA molecule and its five stable fragments within gas phases, ethanol, diethyleter, and chloroform solvents

(Au)	Gases	Ethanol	Diethyleter	Cloroform
CA(ΔE)	-982.131569	-982.147270	-982.143581	-982.144009
ΔH	-982.130624	-982.146326	-982.142637	-982.143065
ΔG	-982.216736	-982.231856	-982.227963	-982.228375
C1	-942.863145	-942.879082	-942.875406	-942.875835
	-942.862201	-942.878138	-942.874462	-942.874891
	-942.943458	-942.959794	-942.956225	-942.956639
C2	-942.846685	-942.862326	-942.858664	-942.859086
	-942.845741	-942.861382	-942.857720	-942.858142
	-942.927852	-942.942980	-942.939834	-942.940154
C3	-903.578350	-903.594172	-903.590523	-903.590944
	-903.577405	-903.593228	-903.589579	-903.589999
	-903.655385	-903.671679	-903.668871	-903.669009
C4	-903.563260	-903.578914	-903.575329	-903.575759
	-903.562316	-903.577969	-903.574384	-903.574815
	-903.640893	-903.656208	-903.652826	-903.653259
C5	-867.651642	-867.665806	-867.662545	-867.662928
	-867.650698	-867.664862	-867.661601	-867.661984
	-867.729172	-867.744299	-867.740470	-867.740894

3.Conclusion

The emergence of C2 fragment was formed by the disintegration of one of these fragments. C2 fragment with its -942.846685 Au energy is the second most stable fragment of CA molecule following C1 fragment. The fragmentation reaction of the CA molecule continues in two different paths after its fragmentation as C1 and C2, which can be seen in Fig. 3.

In Table 1, however, energy values (Au) of CA molecule and its five stable fragments within gas phases, ethanol, diethyleter, and chloroform solvents were given.

When the energy values in various phases of CA and its stable 5 fragments, which are given in Fig. 3, were analyzed, it was determined that every energy value was negative. This revealed that the fragmentation reaction in each phase occurred spontaneously. If solvents would be analyzed, it would be determined that energy values, from the lowest, in other words, the most stable, to the least stable are ethanol, chloroform, diethyleter, and gas phase respectively.

References

[1] Govindarajan VS, Sathyanarayana MN, Capsicum--production, technology, chemistry, and quality. Part V. Impact on physiology, pharmacology, nutrition, and metabolism; structure, pungency, pain, and desensitization sequences. Crit Rev Food Sci Nutr. 1991; 29:435-74.

[2] O'Neill J, Brock C, Olesen AE, Andresen T, Nilsson M, Dickenson AH. Unravelling the mystery of capsaicin: a tool to understand and treat pain. Pharmacol Rev. 2012;64(4):939-71.

[3] Perucka I, Materska M, Phenylalanine ammonia-lyase and antioxidant activities of lipophilic fraction of fresh pepper fruits Capsicum annum L. Innovative Food Science& Emerging Technologies, 2001;2:189-92.

[4] Gaussian 09, Revision B.04, Gaussian, Inc., Pittsburgh: PA, 2009.

[5] Hatipoglu A, Vione D, Yalcin Y, Minero C. and Cinar Z, Photo-oxidative degradation of toluene in aqueous media by hydroxyl radicals. J. Photochem. and Photobiol. 2010; 215:59-68.

[6] Eren B, Yalcin Gurkan Y, Possible reaction pathways of the lincomycin molecule according to the DFT calculation method. JSCS., 2017;82:277-87.

[7] Atkins PW, Physical Chemistry, 6th ed.; Oxford University Press: New York, 1998(ISBN: 9780198769866).

[8] Mierzejewska K, Trylska J, Sadlej J, Quantum mechanical studies of lincosamides. J. Mol. Model. 2012; 18:2727–40.

[9] Diercksen Geerd HF, Sutcliffe BT, Veillard A, Computational Techniques in Quantum Chemistry and Molecular Physics. Proceedings of the NATO Advanced Study Institute held, Ramsau: Germany, 1974, 4.

[10] Parr RG, Yang W, Oxford University Press, New York ,1989.

[11] Koch W, Holthausen MC, WILEYVCH, 2001.

FUNCTIONALIZED CLINOPTILOLITE FOR REMOVAL OF SOLUBLE DYES IN AQUEOUS SOLUTION

Neli MINTCHEVA, Gospodinka GICHEVA, Lyubomir DJERAHOV, Marinela PANAYOTOVA

Department of Chemistry, University of Mining and Geology, 1700 Sofia, Bulgaria

e-mail: nnmintcheva@mgu.bg

Abstract

Among organic pollutants in water soluble dyes are considered as stable, persistent and harmful substances for the environment that require multiple steps of treatment. Various methods have been applied for removal of dyes from wastewater such as adsorption, membrane ultrafiltration, microbiological treatment, electrochemical oxidation, photocatalysis, etc. Recently we have aimed to prepare low-cost and eco-friendly materials based on natural sources that can be used in water treatment. We have chosen composites consisting of ZnO nanoparticles supported onto the zeolite and examined their properties in decolorization of methylene blue (MB). The nanocomposites were synthesized by precipitation of zinc oxalate onto the zeolite followed by thermal decomposition of oxalate to nanosized ZnO loaded on the clinoptilolite. The phase composition, morphology and surface chemistry were studied by set of methods: XRD, SEM, FT-IR, UV-vis. Additionally, we have evaluated the decolorization of MB as a model of water-soluble dye and examined several experimental conditions such as dye concentration, treatment time, adsorbent doses, pH for efficient dye removal.

Key Words: *clinoptilolite; ZnO-Zeolite nanocomposites; dye removal; adsorption; photocatalysis*

1. Introduction

The water soluble dyes are commonly used in various fields such as textile and paper industries, cosmetics, plastics, etc. The release of toxic organic compounds in wastewater can cause serious environmental problems for the ecosystems and human health. One of the widely used methods for pollutants removal is adsorption on natural or synthetic materials. Clinoptilolite is a natural zeolite which is well known adsorbent for many heavy metal cations, while the functionalized clinoptilolites are promising for removal of organic compounds [1,2]. ZnO is considered as capable photocatalyst for photooxidation of organic pollutants. It is biocompatible material that can be applied without any risk for the living organisms. ZnO is a typical semiconductor with a wide band gap of 3.37 eV that is able to absorb a large region of solar spectrum, thus showing high photocatalytic efficiency [3-5]. The motivation for the present work was to prepare nanocomposite that can remove organic pollutants from aqueous solutions by enhanced adsorption of dyes and their degradation onto ZnO under solar light irradiation.

2. Experimental

2.1. Materials

Zinc acetate ($Zn(CH_3COO)_2.2H_2O$), oxalic acid ($H_2C_2O_4.2H_2O$), 96% ethanol and methylene blue were purchased from Teocom Ltd. Natural zeolite from the Rhodope mountain in Bulgaria was used. The preliminary XRD study revealed that the material contains 73% clinoptilolite. The natural zeolite was milled, sieved, fractioned and washed thoroughly as described in our previous paper [6].

2.2. Methods

Preparation of nanocomposite (ZnO/Zeo): First, zinc oxalate was synthesized by mixing 0.005 mol $Zn(CH_3COO)_2.2H_2O$ (1.097 g) and 0.005 mol $H_2C_2O_4.2H_2O$ (0.630 g) in ethanol solution at 50 ^oC for 30 min. Then 0.300 g zeolite were added and the mixture was agitated for 60 min at the same temperature, after which it was cooled down to room temperature and continuously stirred overnight. The solvent was evaporated under vacuum in a rotary evaporator, the residue was dried at 60 ^oC in an oven and annealed at 500 ^oC in a muffle furnace. As described modified procedure was based on the previously reported paper [8].

Methods for characterization of ZnO/Zeo: The prepared composite was characterized by X-ray diffraction analysis (BRUKER D2 Phaser), scanning electron microscopy (SEM/FIB LYRA I XMU from TESCAN), FT-IR and reflectance UV-vis spectroscopy (Nicolet 6700 FTIR spectrometer and Evolution 300 UV-Vis Spectrophotometer, respectively both from Thermo Fisher Scientific). The decolorization tests were carried out by monitoring of the reaction mixture on UV-vis spectrophotometer (Boeco, S-220, UV-vis).

3. Results and discussion

3.1. Characterization of ZnO-Zeo nanocomposite

Fig. 1 shows the XRD patterns of natural clinoptilolite, ZnO and composite ZnO/Zeo. The natural zeolite was washed several times in acidified solutions to remove all soluble salts and clay minerals, and then it was used for the nanocomposite preparation. The XRD patterns of this material shows peaks for clinoptilolite and barrerite that were found to be 73% and 27%, respectively [6,7]. In parallel, pure ZnO was also synthesized according to above described procedure. Its XRD patterns are displayed on Fig. 1. The peaks were indexed as the hexagonal wurtzite structure of ZnO (JCPDS card no. 36-1451). The ZnO/Zeo sample shows the XRD patterns of both ZnO and clinoptilolite phases and it reveals the formation of nanocomposite.

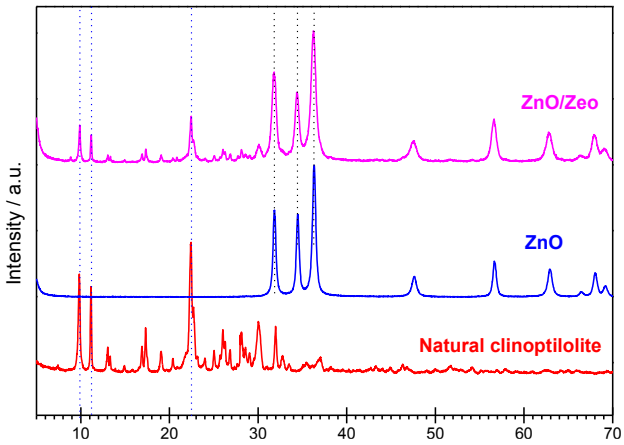

Fig. 1. XRD patterns of natural clinoptilolite, ZnO and composite ZnO/Zeo

The UV-vis spectroscopy was used to confirm the layer of ZnO on zeolite. As a semiconductor ZnO exhibits a plasmon resonance in the UV region. The typical band edge at 375-400 nm can be seen in the UV-vis diffuse reflectance spectra of ZnO and ZnO/Zeo presented on Fig. 2. In the infrared spectrum of nanocomposite ZnO/Zeo the characteristic bands of both phases ZnO, clinoptilolite were observed. The FT-IR spectra of ZnO, clinoptilolite and ZnO/Zeo are shown on Fig. 3. The strong band at 550-500 cm^{-1} in the spectra of ZnO and ZnO/Zeo is assigned to Zn-O bond in the crystal lattice of the oxide. The intensive band at 1200-1000 cm^{-1} in the spectra of clinoptilolite and composite are due to stretching vibrations of Si-O and Al-O bonds in the skeleton of zeolite. The broad and strong bands in the region 3600-3400 cm^{-1} in all spectra give rise from the presence of hydroxyl groups and adsorbed water molecules.

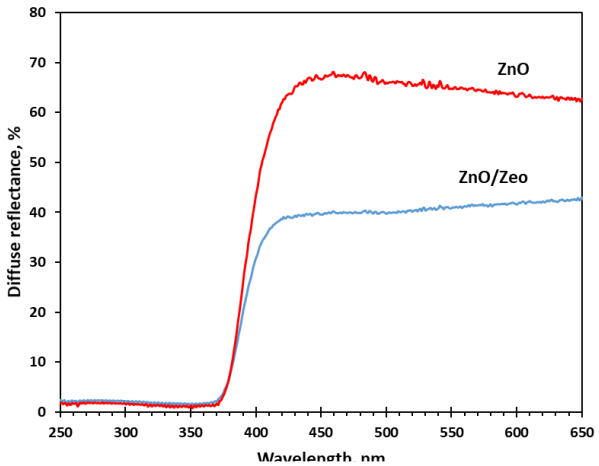

Fig. 2. UV-vis diffuse reflectance spectra of ZnO and ZnO/Zeo

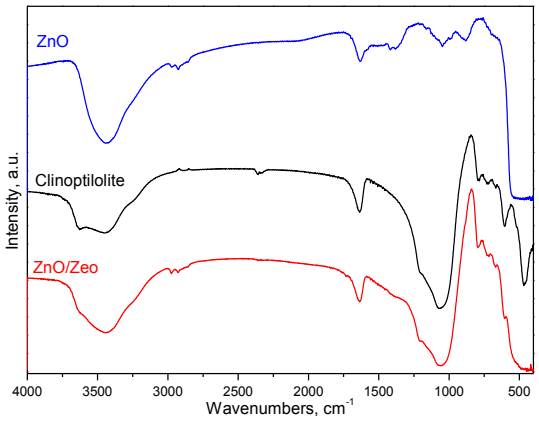

Fig. 3. Infrared spectra of ZnO, clinoptilolite and nanocomposite ZnO/Zeo

The morphology of the nanocomposite was evaluated by SEM analysis. On Fig. 4 are displayed SEM images of the composite at low and high magnification. The zeolite particles are in the range from 2 to 20 μm and

have different shapes. They are covered with even and steady layer of ZnO. It crystalized in cotton-like nanothread in the process of thermal decomposition of zinc oxalate to zinc oxide.

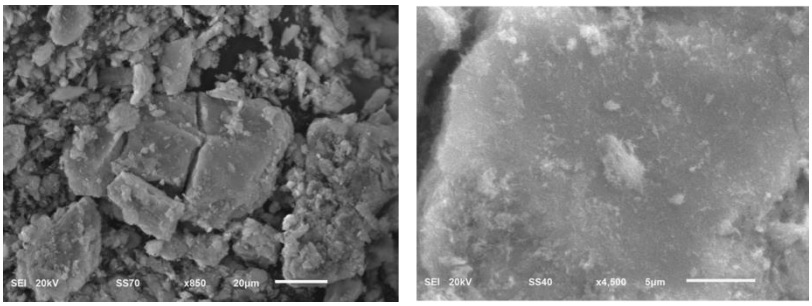

Fig. 4. SEM images of the nanocomposite ZnO/Zeo

3.2. Adsorption ability of ZnO/Zeo nanocomposite

The prepared nanocomposite was tested for removal of methylene blue (MB) as a model compound of soluble dye in aqueous solution. The change in methylene blue concentration was monitored by UV-vis measurement of intensity of the absorption band at wavelength 664 nm, which is characteristic for this dye. The evaluation of the decolorization of methylene blue solution was carried out at different conditions. The effect of the nanocomposite doses in the range 0.05-0.30 g on the decolorization efficiency of MB is shown on Fig. 5. As the dose of ZnO/Zeo increases the decolorization efficiency increases. The dose of 0.30 g composite per 50 mL MB solution with concentration 10 mg/L allows to remove 80% of the dye for 30 min and around 93% for 60 min. After that the rate of adsorption remains almost constant with increasing the time.

The effect of MB concentration on the decolorization was tested by using of 0.10 g composite in 50 mL solution of MB in the concentration range 4-10 mg/L. At concentration 4 mg/L of MB, 90% removal was achieved for 20 min (see Fig. 6). Increasing the concentration of the dye twice leads to decreasing of the efficiency to half. The decolorization degree at 8 and 10 mg/L MB is very similar indicating that the adsorption ability of the composite reached the maximum.

The effect of pH on the adsorption of MB onto composite was also investigated. In alkaline solution the decolorization efficiency of the MB slightly increases in comparison with the initial pH of MB solution (pH 4.2). It was found that for 60 min around 10% more MB is adsorbed in alkaline solution than that in acidic medium. Nevertheless, this result did not satisfy us and all other tests described above were carried out without additional adjustment of pH of solution.

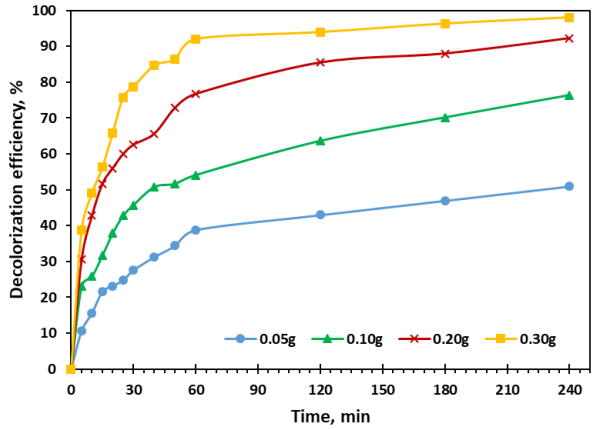

Fig. 5. Effect of nanocomposite doses on the MB removal

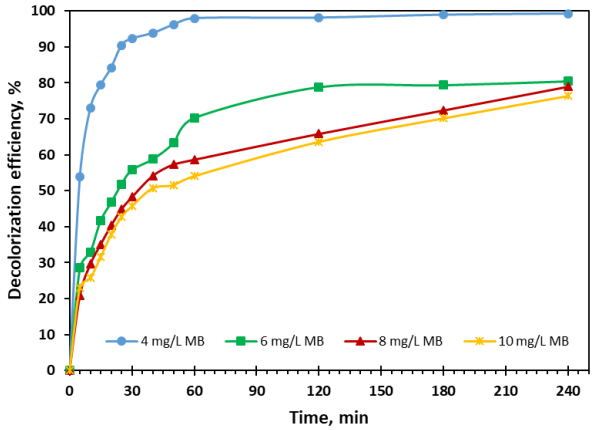

Fig. 6. Effect of MB concentration on the decolorization efficiency

4. Conclusions

In this paper we reported preparation of functionalized clinoptilolite, ZnO/Zeo by precipitation and deposition of zinc oxalate on zeolite and subsequent thermal decomposition of oxalate to ZnO loaded on the clinoptilolite. A nanomaterial with nanothread morphology of ZnO onto micro-sized zeolite crystals was obtained. The ZnO/Zeo composite was tested in removal of water-soluble organic compounds such as MB dye and it demonstrated good adsorption properties. Thus the synthesized low-cost and eco-friendly material based on

natural zeolite might be used in water treatment and removal of organic compounds. Adsorption of MB over nanocomposites and/or its photocatalytic degradation onto ZnO incorporated in the nanocomposites are promising for minimization of the adsorbent waste and its reusability.

Acknowledgements

This work is part of the project "Functional composite nanomaterials obtained from natural resources for environment protection" funded by the Bulgarian National Science Fund, contract No DH 17/20–2017.

References

[1] Sayed M.A.A., Khater M.S., 2013. Removing Cadmium and Lead From Wastewater Using Natural Zeolite Isotherm models. *Middle East Journal of Applied Sciences* 3(3), p. 98-104.

[2] Margeta K., Logar N.Z., Šiljeg M., Farkaš A., Natural Zeolites in Water Treatment – How Effective is Their Use. Chapter 5. Intech. 2013. http://dx.doi.org/10.5772/50738.

[3] Kołodziejczak-Radzimska A., Jesionowski T., 2014. Zinc Oxide—From Synthesis to Application: A Review. *Materials*, 7, p. 2833-2881.

[4] Kumari V., Mittal A., Jindal J., Yadav S., Kumar N., 2019. S-, N- and C-doped ZnO as semiconductor photocatalysts: A review. *Front. Mater. Sci.* 13, p. 1-22.

[5] Qi K., Cheng B., Yu J., Ho W., 2017. Review on the improvement of the photocatalytic and antibacterial activities of ZnO. *J. Alloys Comp.* 727, p. 792-820.

[6] Panayotova M., Mintcheva N., Djerahov L., Gicheva G., 2018. Kinetics and thermodynamics of silver ion immobilisation by natural clinoptilolite. *Journal of mining and geological sciences*, Part II, 61, p.87-91.

[7] Panayotova M., Mintcheva N., Gemishev O., Tyuliev G., Gicheva G., Djerahov L., 2018. Preparation and antimicrobial properties of silver nanoparticles supported by natural zeolite clinoptilolite. *Bulg. Chem. Commun*., 50 (F), p. 211–218.

[8] Chung Y. T., Ba-Abbad M.M., Mohammad A. W., Hairoma N.H.H., Benamor A., 2015. Synthesis of minimal-size ZnO nanoparticles through sol–gel method: Taguchi design optimisation. *Materials and Design* 87, p. 780–787.

PREPARATION OF SILVER NANOPARTICLES AND NANOCOMPOSITE SILVER NANOPARTICLES-ZEOLITE BY CHEMICAL REDUCTION AT ROOM TEMPERATURE

Neli MINTCHEVA, Gospodinka GICHEVA, Marinela PANAYOTOVA, Lyubomir DJERAHOV

Department of Chemistry, University of Mining and Geology, 1700 Sofia, Bulgaria

e-mail: nnmintcheva@mgu.bg

Abstract

In this study we present a method for synthesis of composite material consisting of AgNPs and natural zeolite. The procedure involves sorption of silver ions onto zeolite followed by chemical reduction of ions to silver nanoparticles. The reduction is conducted at room temperature using sodium citrate as a green reagent. The reaction is catalyzed by an amine, monoethanolamine (MEA) or triethanolamine (TEA), which allows to lower the reaction temperature. Using this modified citrate method we have obtained AgNPs in solution and AgNPs-zeolite nanocomposite materials.

Key Words: nanotechnology; silver nanoparticles; environmental protection; AgNPs –zeolite; nanocomposite

1. Introduction

Silver has been long known for its antibacterial activity and silver nanoparticles, AgNPs, are widely used in many modern fields of nanotechnology – catalysis, microbiology, electronics, and environmental protection [1]. AgNPs possess unique physical and optical properties. In order to improve their stability and make them more accessible they are often immobilized onto some support – natural (zeolite [2], clay [3], silica) or synthetic (polymers matrix, beads and fibres [4]), thus forming a nanocomposite material. This way their application in environmental protection is much more convenient, long-lasting and cost effective.

A lot of research work is available on the implementation of silver onto biocompatible and biodegradable materials such as chitosan [5] and cellulose [6]. These materials have shown excellent results for membranes in reverse osmosis [7].

In this paper we show low-temperature reduction of silver ions in solution as well as Ag^+ immobilized onto zeolite in the presence of amine and fabrication of both bare AgNPs and nanocomposite AgNPs-zeolite. These materials have been characterized by UV-vis spectroscopy and transmission electron microscopy.

2. Experimental part

2.1. Materials

Silver nitrate salt (purum >99,8%) was purchased from Teokom Ltd (Bulgaria), tri-sodium citrate dihydrate ($Na_3Cit.2H_2O$; for analysis) from MERCK&CO., monoethanolamine (MEA; pure p. a.) and triethanoloamine (TEA; pure p. a.) were delivered by POCH™ (Poland). The surfactant used in the experiments – PVP (polyvinylpyrrolidone, M.W. 40,000) was purchased from Alfa Aesar. All reagents were used without further purification. All the solutions were made using double distilled water. The zeolite used in the experiments has natural origin from the region of Rhodopes Mountain, Bulgaria. It was subjected to treatment consisting of milling, sieving and washing before its use.

2.2. Materials characterization

The silver nanoparticles (AgNPs) obtained in solution were characterized by UV-Vis spectral analysis performed on BOECO, model S-220 UV/Vis. The recorded spectra showed peaks characteristic for AgNPs. The size and the morphology of the silver nanoparticles in solution and in composite material was estimated with the use of transmission electron microscopy (TEM) – JEOL model JEM 2100 200kV.

2.3. Methods

Preparation of AgNPs in solution

Silver nitrate was dissolved in double distilled water (d.d. H_2O) on constant magnetic stirring at room temperature. A solution of PVP with different concentrations (Table 1) was added to the $AgNO_3$ solution dropwise and the reaction mixture was stirred for 30 minutes. A solution of Na_3Cit (2.10^{-3} M; 20 ml) was then

introduced to the mixture also dropwise followed by the addition of 3 ml solution of catalyst MEA (or TEA). All of the reagent concentration and samples' numbers are depicted in Table 1.

Table 1. Concentrations (in mol/l) of reagents used in the preparation of AgNPs and the corresponding number of the sample as used in text

Sample	17-1	17-2	19-1	19-2	23-1	23-2	24-1	24-2	25-1	25-2
Ratio[1]	1:1	1:1	1:1	1:1	2:1,5	2:1,5	1,5:2	1,5:2	1:2	1:2
$AgNO_3$	2.10^{-3}	2.10^{-3}	2.10^{-3}	2.10^{-3}	2.10^{-3}	2.10^{-3}	$1,5.10^{-3}$	$1,5.10^{-3}$	1.10^{-3}	1.10^{-3}
Na_3Cit	2.10^{-3}	2.10^{-3}	2.10^{-3}	2.10^{-3}	$1,5.10^{-3}$	$1,5.10^{-3}$	2.10^{-3}	2.10^{-3}	2.10^{-3}	2.10^{-3}
TEA-1	2.10^{-5}		3.10^{-5}		3.10^{-5}		3.10^{-5}		3.10^{-5}	
MEA-2		2.10^{-5}		3.10^{-5}		3.10^{-5}		3.10^{-5}		3.10^{-5}

[1] ratio $AgNO_3$ to Na_3Cit

Preparation of AgNPs-zeolite composite

The nanocomposite material was prepared utilizing the procedure for AgNPs synthesis in solution. Ag^+ ions were immobilized onto zeolite surface by immersing zeolite powder in silver nitrate solution at room temperature. After 4 h the zeolite powder was filtered and washed with distilled water until negative reaction for silver ions. The wet Ag^+-zeolite was dispersed in sodium citrate solution and then TEA/MEA was added to this reaction mixture. The dispersion was left for 24 h at room temperature in dark chamber for the reduction of silver ions to silver nanoparticles to take place. As obtained nanocomposite material was filtered and washed with distilled water and dried in vacuum desiccator. Then the obtained powder was submitted to different analyses for their structure and composition determination.

3. Results and discussions

3.1. Characterization of AgNPs in solution

Synthesis of silver nanoparticles in our study was based on a modification of citrate method consisting of use of catalyst. It allowed the reaction to be conducted at room temperature which is of importance for the preparation of nanocomposite material. A several reaction parameters were investigated – the type of the catalyst, its concentration, the effect of surfactant addition and the initial ratio of the reagents.

In Fig. 1(a, b) are shown the absorption spectra of the resulting AgNPs in solution obtained at different reaction conditions. All of them display the characteristic maximum attributed to the formation of nano-silver. When comparing the spectra of samples **23-1**, **24-1** and **25-1** one can see that they have similar broad peak with maxima at 430 nm. These samples have different initial ratio of $AgNO_3$ to Na_3Cit and TEA as catalyst (all other parameters are constant). Sample **23-1** has excess of silver ions which can't be completely reduced so the yield of AgNPs is low and the size distribution is broad. When increasing the amount of citrate (sample **24-1** and **25-1**), which plays the role of reducer, the conversion is greater and the yield is higher. Despite that the peak remains broad, indicating broad size distribution.

When we use MEA as a catalyst – samples **23-2, 24-2** and **25-2**, the opposite trend is observed – the intensity of the maxima decreases with the increase of citrate concentration (ratio) and the peak broadens. This observation can be related to the fact that the reaction rate is faster when the reaction is catalyzed by MEA (in comparison with TEA) so quick formation of silver nanoclusters occurs with well pronounced maxima at 420 nm (sample **23-2)** (Fig. 1a). When the amount of citrate is increased (samples **24-2** and **25-2**) the degree of conversion decreases and smaller fraction of nano silver is formed with broad maximum – Fig. 1a.

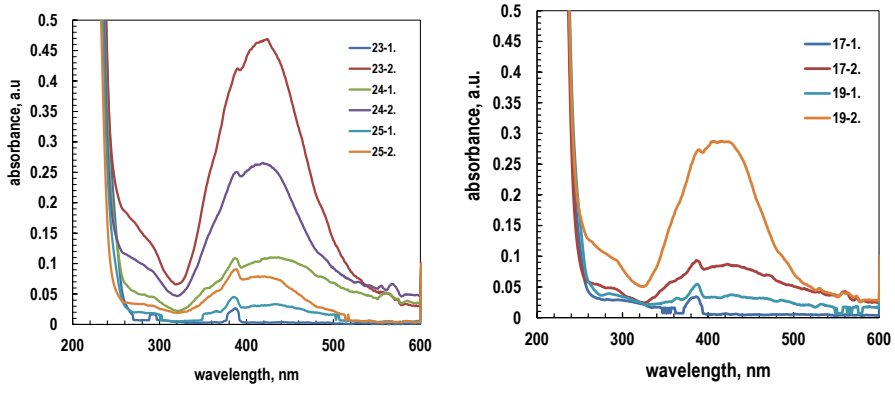

(a) (b)

Fig. 1. UV-spectra of the Ag NPs, obtained in the presence of different initial ratio of $AgNO_3$ to Na_3Cit (a) and different amount of catalyst (b)

In Fig. 1b the effect of catalyst concentration is demonstrated by comparison of the absorbance spectra of AgNPs obtained in solution. In samples denoted as **17-1, 17-2, 19-1** and **19-2** is investigated the effect of TEA and MEA concentration – all other parameters are kept constant (Table 1). When comparing the spectra of sample **19-1** and **19-2** we can surmise that at these reaction conditions MEA is the more suitable catalyst then TEA (Fig. 1b). When the concentration of MEA is increased the intensity of the absorption maximum also increases (sample **17-2** and **19-2**) which is an indication that reaction rate is accelerating. The AgNPs of sample 19-2 shows well pronounced peak with maximum at 420 nm.

The TEM image of sample 23-2 shown in Fig. 2 represents silver nanoparticles having plate-like shape with average size about 40 nm.

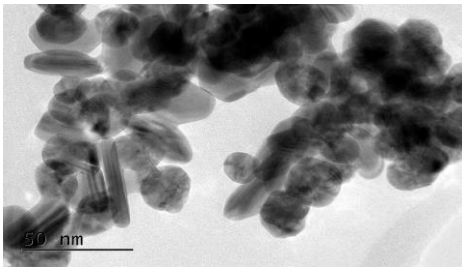

Fig. 2. TEM images of the Ag NPs, obtained in the presence of MEA (sample 23-2)

3.2. Characterization of AgNPs-zeolite composite

The obtained nanocomposite material in form of powder was analyzed by transmission electron microscopy (TEM). The images revealed that the reduction of silver ions immobilized onto zeolite surface was successful and AgNPs were formed (Fig. 3).

Images in Fig. 3 show that the AgNPs are evenly distributed on the zeolite surface and have an average size of about 5nm (Fig. 3b) and single particles with size of 40 nm (Fig. 3a) are also observed. Thus prepared AgNPs -zeolite nanocomposites have been used in some preliminary tests against *E. coli* as a potential antibacterial material and have shown promising results.

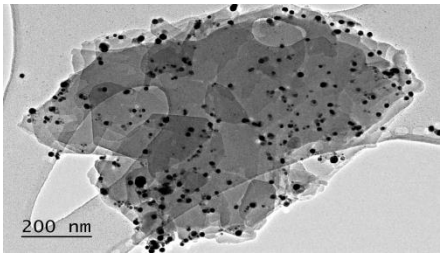

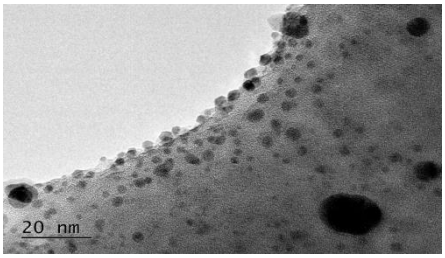

(a) (b)

Fig. 3. TEM images of the Ag NPs-zeolite composite material, obtained by reduction of silver ions, immobilized on the zeolite, in the presence of TEA as catalyst at lower (a) and higher magnification (b)

4. Conclusions

It was shown that the modification of citrate methods can be successfully utilized for the preparation of AgNPs at room temperature. Both of the tested amine catalysts demonstrated activity in the process of reduction of silver ions. UV-vis spectra and TEM analyses confirmed the formation of nanoclusters of silver. The absorbance spectra showed that the presence of MEA leads to formation of smaller AgNPs which continue to grow, forming bigger ones. This can be related to the slight red shift of the peak of 19-2 compared to 17-2. Other parameter affecting the process is silver ion concentration - the higher its initial concentration is the faster is the formation of more uniform in size AgNPs.

A nanocomposite material was prepared at room temperature by chemical reduction. Two types of amine catalyst were applied – TEA and MEA. TEM analysis revealed that the AgNPs with average size of 5 nm are

obtained and uniformly distributed onto the zeolite surface. A small fraction of AgNPs with average size of 40 nm is also present. Thus prepared nanocomposite material is in suitable form for application in water treatment.

Acknowledgements

This research was funded by Bulgarian National Science Fund contract No DH 17/20–2017. The experiments and the results are part of the ongoing research done in project "Functional composite nanomaterials obtained from natural resources for environment protection".

References

[1] Saengmee-anupharb S, Srikhirin T, Thaweboon B, Thaweboon S, Amornsakchai T, Dechkunakorn S, Suddhasthira T. Antimicrobial effects of silver zeolite, silver zirconium phosphate silicate and silver zirconium phosphate against oral microorganisms. Asian Pac J Trop Biomed 2013; 3(1):47-52.

[2] Jiraroj D, Tungasmita S, Tungasmita D. N. Silver ions and silver nanoparticles in zeolite: A composites for antibacterial activity. Powder Technol. 2014; 264; 418–422.

[3] Sprynskyy M, Sokol H, Rafińska K, Brzozowska W, Railean-Plugaru V, Pomastowskic P, Buszewskia B. Preparation of AgNPs/saponite nanocomposites without reduction agents and study of its antibacterial activity. Colloids Surf., B. 2019; 180; 457–465

[4] Parmar A, Kaur G, Kapil S, Sharma V, Sachar S, Sandhir R, Sharma S. Green chemistry mediated synthesis of PLGA-Silver nanocomposites for antibacterial synergy: Introspection of formulation parameters on structural and bactericidal aspects. React. Funct. Polym. 2019; 141; 68-81

[5] Maruthupandy M, Rajivgandhi G, Muneeswaran T, Vennila T, Quero F. Song J. M. Chitosan/silver nanocomposites for colorimetric detection of glucose molecules.2019; 121; 822-828.

[6] Muthulakshmi L, Rajini N, Rajalu A.V, Siengchin S, Kathiresan T. Synthesis and characterization of cellulose/silver nanocomposites from bioflocculant reducing agent. Int. J. Biol. Macromol. 2017; 103;1113-1120.

[7] Wua J, Yua C, Li Q. Novel regenerable antimicrobial nanocomposite membranes: Effect of silver loading and valence state. J. Membr. Sci. 2017; 531; 68–76.

Structure/Reactivity Properties of Manganese-Based Imidazole Complexes: A DFT Study

Gaye GÜNGÖR[1], Dolunay ŞAKAR DAŞDAN[1], Elvan ÜSTÜN[2]

[1] Department of Chemistry, Faculty of Art and Science, Yıldız Technical University, 34220 Istanbul, Turkey; dolunaykar@yahoo.com

[2] Department of Chemistry, Faculty of Art and Science, Ordu University, 52200 Ordu, Turkey

Abstract

In order to utilize the bioactivities of carbon monoxide which are known to be endogenously synthesized in the body, the molecules that store and carry carbon monoxide have to be synthesized/characterized. The most commonly used molecules for this purpose are metal carbonyl complexes. The use of DFT-based calculation methods for determining the most appropriate molecule provides several advantages rather than synthesis/analysis procedures. In this study, local reactivity descriptors and electronically intense regions of synthesized/characterized $[Mn(CO)_3L(bpy)]^+$ {bpy:2,2'-bipyridyl; L: imidazole **(1)**, methylimidazole **(2)**} molecules were calculated.

Key Words: *Local Reactivity Descriptors, DFT/TDDFT, Manganese Carbonyl Complexes*

1. Introduction

Carbon monoxide, which is known as a colorless, odorless, toxic is defined as a gasotransmitter [1]. The studies confirm the many activities of carbon monoxide such as vasodilatory, anti-bacterial and anti-cancer [2-4]. The molecules which synthesize for storage and carrying carbon monoxide independent from toxic properties are called "CO-releasing molecules (CORMs)" [5]. Although the various organic species have been synthesized/tested, the most important CORMs are metal carbonyl complexes [6]. For this purpose, many carbonyl complexes were synthesized, and CO-releasing properties were investigated [7–9] .

The CO releasing properties of a metal carbonyl complex has been affected by the type of metal and non-carbonyl ligand. In order to determine the most suitable carbonyl complex, dft-based calculation methods for analyzing possible complexes saves work, labor and material. Global and local reactivity descriptors are accepted appropriate criteria for making theoretical interpretations on the activity of molecules.

In this study, synthesized/characterized $[Mn(CO)_3L(bpy)]^+$ {bpy:2,2'-bipyridyl; L: imidazole **(1)**, methylimidazole **(2)**} were optimized by ORCA package [10] and the local reactivity descriptors of the molecules were calculated [11, 12].

2. Calculation Method

DFT/TDDFT calculations for full unconstrained geometry optimizations tricarbonyl complexes were carried out with ORCA version 3.0.3 using BP86 exchange functional with the resolution-of-the-identity (RI) approximation, a TZVP basis set and the tightscf and grid4 options [7, 9 ,10]. The COSMO solvation model was used for analyzing the solvent effects on all calculations. To speed up the calculations, TZVP/J auxiliary basis set was used. Local reactivity descriptors were also calculated by using HOMO and LUMO energies of optimized one-electron-added form and one-electron-removed form of molecules. "ElDens" option of the ORCA package was used for the electron density calculations and gOpenMol was used for all the graphical illustrations. Local reactivity descriptors of the molecules were calculated with the method that provided Hazarika et al [11, 12].

3. Result and Discussion

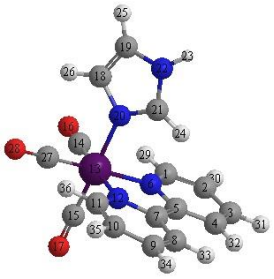

Table 1. Local reactivity descriptors of **1** in acetonitrile and gas phase (**bold**: the most active atoms)

	gas			acetonitrile		
	$f^{(-)}$	$f^{(+)}$	$f^{(0)}$	$f^{(-)}$	$f^{(+)}$	$f^{(0)}$
C_2	**0.068**	0.008	0.038	**0.088**	0.008	0.048
C_4	**0.052**	0.015	0.034	**0.065**	0.012	0.039
C_8	**0.052**	0.016	0.034	**0.065**	0.012	0.038
C_{10}	**0.068**	0.007	0.038	**0.088**	0.008	0.048
O_{16}	**0.069**	**0.112**	**0.091**	0.046	**0.115**	**0.080**
O_{17}	**0.060**	**0.143**	**0.102**	0.039	**0.171**	**0.105**
N_{20}	-0.008	**0.079**	0.035	0.006	**0.113**	**0.060**
O_{28}	**0.069**	**0.111**	**0.090**	0.046	**0.114**	**0.080**

Fukui function, which is defined for the investigation of the local reactivity of the molecules from hard-soft acid base theory, is considered as a measurement of the repercussion to nucleophilic / electrophilic / radicalic attacks of a specific region of molecules. The atom with big Fukui value should be considered the most active site of the molecule against the chemically attack.

Fukui functions of studied molecules for nucleophilic ($f^{(+)}$), electrophilic ($f^{(-)}$) and radicalic ($f^{(0)}$) attacks both in gas form and in acetonitrile are given in the Table 1 and Table 2. It can be seen from the calculations of the complex **1** for the electrophilic attack that the most active atom of the molecule in the gas phase are oxygen of the equatorial carbonyl ligand while oxygen of the axial carbonyl is expected to have a considerable electrophilic activity. However, the oxygens of the carbonyls are not as effective as the carbons in the meta position of the bipyridyl for the electrophilic attack in acetonitrile. In terms of nucleophilic attack, the Fukui function values of complex **1** in gas phase and acetonitrile are more compatible with each other than that of for electrophilic calculations. In both cases, the most sensitive region of the molecule to the nucleophilic attack is the carbonyl oxygens. Furthermore, nitrogen, which links the imidazole to the manganese, is very effective against nucleophilic attacks. The active sites of the complex **2** against nucleophilic ($f^{(+)}$), electrophilic ($f^{(-)}$) and radicalic ($f^{(0)}$) attacks are could be also seen in Table 2.

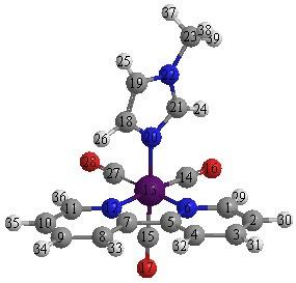

Table 2. Local reactivity descriptors of **2** in acetonitrile and gas phase (**bold**: the most active atoms)

	gas			acetonitrile		
	$f^{(-)}$	$f^{(+)}$	$f^{(0)}$	$f^{(-)}$	$f^{(+)}$	$f^{(0)}$
C_2	**0,066**	0,014	0,040	**0,086**	0,004	0,045
C_4	0,048	0,014	0,031	**0,060**	0,016	0,038
C_8	0,047	0,010	0,028	**0,061**	0,016	0,039
C_{10}	**0,069**	-0,003	0,033	**0,091**	0,002	0,047
N_{12}	0,023	**0,086**	**0,054**	0,022	0,027	0,025
O_{16}	**0,067**	**0,112**	**0,090**	0,047	**0,121**	**0,084**
O_{17}	**0,060**	**0,136**	**0,098**	0,039	**0,140**	**0,089**
N_{20}	0,012	**0,070**	0,041	0,016	**0,119**	0,068
O_{28}	**0,067**	**0,099**	**0,083**	0,046	**0,116**	**0,081**

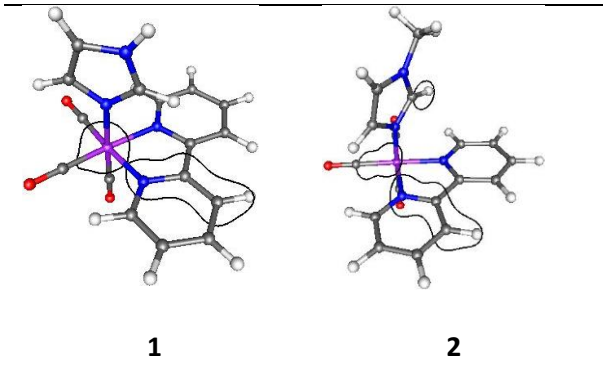

1 **2**

Fig 1. Electron density of the molecules

The electrostatic interactions between charged chemical particles and the charges in suspension effects the formation of sliding surface. It is thought that theoretical determination of the high electron density regions could give insight into the analysis of the electronic and electrostatic interactions of the molecules. Linear electron density illustrations of optimized molecules which achieved by using DFT based calculation methods are given in Fig. 1. The electron density is observed on the bipyridyl ring in all molecules while the electron density on manganese have shifted toward the equatorial carbonyl with the enlargement of the ligand volume. Furthermore, the regions where the electrons are condensed on the molecule vary when the ligand is getting larger.

Acknowledgements

Support of Scientific and Technological Research Council of Turkey (TÜBİTAK, Project No 112T320) is gratefully acknowledged.

References

[1] Wegiel B, Hanto DW, Otterbein LE. The social network of carbon monoxide in medicine Trends Mol. Med. 2013; 19:3–11.

[2] Motterlini R, Haas B, Foresti R. Emerging concepts on the anti-inflammatory actions of carbon monoxide-releasing molecules (CO-RMs). Med. Gas Res. 2012;2:28.

[3] Wareham LK, McLean S, Begg R, Rana N, Ali S, Kendall JJ, Songuinetti G, Mann BE, Poole RK. The Broad-Spectrum Antimicrobial Potential of [Mn(CO)4(S2CNMe(CH2CO2H))], a Water-Soluble CO-Releasing Molecule (CORM-401): Intracellular Accumulation, Transcriptomic and Statistical Analyses, and Membrane Polarization Antioxid. Redox Signal. 2017;28:1286-1308.

[4] Üstün E, Özgür A, Coşkun F, Demir S, Özdemir İ, Tutar Y. CO-releasing properties and anticancer activities of manganese complexes with imidazole/benzimidazole ligands J. Coord. Chem.2016;69:3384–3394.

[5] Sawle P, Hammad J, Fairlamb IJS, Moulton B, O'Brien CT, Lynam JM, Duhme-Klair AK, Foresti R, Motterlini R. Bioactive properties of iron-containing carbon monoxide-releasing molecules J. Pharmacol. Exp. Ther.2006;318:403–410.

[6] Pierri AE, Pallaoro A, Wu G, Ford PC. A luminescent and biocompatible PhotoCORM J. Am. Chem. Soc. 2012;134:18197–18200.

[7] Kunz PC, Huber W, Rojas A, Schatzschneider U, Spingler B. Tricarbonylmanganese(I) and -rhenium(I) complexes of imidazol-based phosphane ligands: Influence of the substitution pattern on the CO release properties Eur. J. Inorg. Chem. 2009;4:5358–5366.

[8] Jiang X, Chen L, Wang X, Long L, Xiao Z, Liu X. Photoinduced Carbon Monoxide Release from Half-Sandwich Iron(II) Carbonyl Complexes by Visible Irradiation: Kinetic Analysis and Mechanistic Investigation Chem. - A Eur. J. 2015;21:13065–13072.

[9] McLean S, Begg R, Jesse HE, Mann BE, Sanguinetti G, Poole RK. Analysis of the bacterial response to Ru(CO)3Cl(Glycinate) (CORM-3) and the inactivated compound identifies the role played by the ruthenium compound and reveals sulfur-containing species as a major target of CORM-3 action Antioxid. Redox Signal. 2013;19:1999–2012.

[10] Neese F. A critical evaluation of DFT, including time-dependent DFT, applied to bioinorganic chemistry J. Biol. Inorg. Chem. 2006;11:702–711.

[11] Hazarika KK, Baruah NC, Deka RC. Molecular structure and reactivity of antituberculosis drug molecules isoniazid, pyrazinamide, and 2-methylheptylisonicotinate: A density functional approach Struct. Chem. 2009;20:1079–1085.

[12] Neese F. The ORCA program system Wiley Interdiscip. Rev. Comput. Mol. Sci. 2012;2:73–78.

CO-Releasing Properties and Local Reactivity Descriptors of New [Re(CO)$_3$(benzylbenzimidazole)(bpy)]OTf

Elvan ÜSTÜN[1]

[1] Department of Chemistry, Faculty of Science, Ordu University, Turkey

Abstract

Metal carbonyl complexes are one of the most important molecules of organometallic chemistry due to their catalytic activity and unique spectroscopic properties. The using of these complexes as CO-releasing molecules is one of the most important research areas in recent years. One of the most important areas of recent chemical/physical researches is the theoretical investigation of the properties of molecules by using the programs which is designed for this purpose. Thanks to these programs, many structural and reactivity characteristics of the molecules can be analyzed successfully. One of the criteria of this theoretical analysis is the Fukui functions, which enable to investigate the activity of each atom of molecules. In this study, synthesized/characterized [Re(CO)$_3$(benzylbenzimidazole)(bpy)]OTf were optimized by ORCA package and the local and global reactivity descriptors of the molecules are calculated.

Key Words: *Local Reactivity Descriptors, Global Reactivity Descriptors, DFT/TDDFT, Rhenium Carbonyl Complexes*

1. Introduction

Metal carbonyl complexes are considered as one of the most important molecular species of organometallic chemistry [1, 2]. Besides its known catalytic activity, metal carbonyls continue to attract attention due to its biological activity in recent years [3, 4]. The popularity of metal carbonyls has increased thanks to both the usage indirectly in activity measurements owing to their unique spectroscopic properties and their own biological activities [5, 6]. Metal carbonyl complexes have also been used as CO-releasing molecule (CORM) since 2000s [7–9].

The recent developments about DFT/TDDFT-based calculation methods have provided labor, money and time saving with the interpretation of structure/activity relations. In the past, it was possible to make optimization for analyzing structural properties such as bond angles and bond lengths. However, nowadays, it is possible to obtain predictions about bioactivity without synthesizing and characterizing the molecules. In this case, it is possible to synthesize the most appropriate molecule for requirements. These advantages are the incentive force for developing new functions in existent programs and designing new software [10–12].

DFT-based global reactivity descriptors are accepted as useful criteria for estimation of structure / property correlation of the molecules. The obtained HOMO and LUMO energies are used to calculate the ionization potential (IP), electron affinity (EA) and electronegativity (χ) of the molecule. In addition, global softness (S) and chemical hardness (η) provides idea about the reactivity of molecules. The stability of a molecule decreases with increasing global softness of a molecule. Chemical hardness is just the reciprocal of global softness, so the higher the hardness, the lower the reactivity. The electrophilicity index (ω) is an indication of the electrophilic strength of the molecular system against a nucleophile [13].

Since two molecules react each other, one molecule behaves as an electrophile while the other acts as a nucleophile. Roy et al. identified two types of local reactivity descriptors for relative electrophilicity $f^{(-)}$ and relative nucleophilicity $f^{(+)}$ [13, 14]. Fukui functions, which calculates with the charges of each atom, are considered as a measurement of intramolecular and intermolecular reactivity trends of atoms.

In this study, synthesized/characterized [Re(CO)$_3$(benzylbenzimidazole)(bpy)]OTf {bpy:2,2'-bipyridyl; OTf: SO_3CF_3} were optimized by ORCA package [15–18] and the local and global reactivity descriptors of the molecules are calculated.

2. Calculation Method

DFT calculations were carried out with ORCA version 4.1.1 using the BP86 functional with the resolution-of-the-identity (RI) approximation, a TZV/ TZV/J basis set, the tightscf and grid4 options. Local and global reactivity descriptors of the molecules were calculated with the method that provided Hazarika et al [13].

3. Result and Discussion

The global reactivity descriptors which are calculated with HOMO and LUMO energies of molecules for the structure/reactivity evaluations of the molecules are the values such as ionization potential (IP), electron affinity (EA) and electronegativity (χ). In this study, besides the gas phase of the molecule, the theoretical calculations were made in acetonitrile and DMSO, which are often used as solvents in bioactivity analyzes. IP, EA and χ values of the molecule in solution are considerably lower than the gas phase according to the detailed results in Table 1. It can be considered as an appropriate approach to the analyzing the solvent effect in the evaluation of DFT-based calculations. In addition, Global softness (S), chemical hardness (η) and electrophilicity index are recently recommended as a reactivity index. The higher global softness means that lower stability of the molecules and the higher global hardness means also that lower reactivity. In this case, according to the values in Table 1, the molecule is more reactive in acetonitrile. The electrophilicity index is defined as the electrophilic strength of the molecule against a nucleophile, and consistent with other descriptors, the molecule should be considered more electrophilic in acetonitrile.

Table 1. Global Reactivity Descriptors of [$Re(CO)_3$(benzylbenzimidazole)(bpy)]OTf.

	IP	EA	χ	μ	η	S	ω
gas	8.415	6.539	7.477	-7.477	0.938	0.533	29.798
acetonitrile	6.058	3.740	4.899	-4.899	1.159	0.431	10.344
DMSO	6.037	3.712	4.874	-4.874	1.162	0.430	10.215

Fukui Functions which described from the hard-soft acid-base theory are local reactivity descriptors that are shown f (+), f (-) and f (0) as the definition of the reaction of each atom to nucleophilic, electrophilic and radicalic attacks, respectively. The atom with a high Fukui Function value is more active against chemical attacks. In this study, the optimizations of doublet +2 and 0 oxidation states of singlet Re^{+1} complex were tried, but the complex with +2 oxidation state weren't converge and the Fukui functions for the electrophilic and radicalic attack could not be calculated. However, the Fukui functions for the nucleophilic attack were calculated in gas, acetonitrile and DMSO by using both the Mulliken charges and Loedwin charges and given in Table 2. The most active regions of the molecule against nucleophilic attacks in the gas phase calculations are listed as $C_8>C_{10}>H_{41}>H_{44}>O_{17}>O_{16}>C_1>C_2>\dots$ with Mulliken charges while listed as $C_2>C_{10}>C_3>C_9=O_{38}>N_6>O_{16}>C_5\dots$ with Loedwin charges. On the other hand, the reactivity of complex in acetonitrile is collated as $C_4>C_2>C_{10}>C_{37}\dots$ with Mulliken charges. The other arrangements of active sites of the molecules could be analyzed in Table 2.

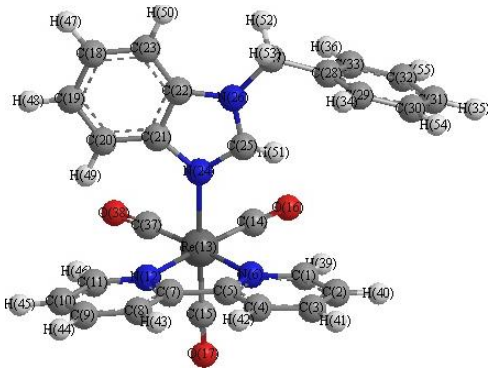

Table 2. Local reactivity descriptors of $[Re(CO)_3(benzylbenzimidazole)(bpy)]OTf$ in acetonitrile, DMSO and gas phase (**blue**: the most active atoms)

Atoms	$f_1^{(-)}$ (gas phase)	$f_2^{(-)}$ (gas phase)	$f_1^{(-)}$ (acetonitrile)	$f_2^{(-)}$ (acetonitrile)	$f_1^{(-)}$ (DMSO)	$f_2^{(-)}$ (DMSO)
C_1	**0,042**	0,026	0,037	0,029	0,037	0,029
C_2	**0,040**	**0,080**	0,061	**0,074**	**0,061**	**0,074**
C_3	0,033	**0,064**	0,046	**0,071**	0,046	**0,071**
C_4	0,039	0,026	**0,076**	0,037	**0,076**	0,037
C_5	-0,001	**0,050**	0,010	**0,056**	0,010	**0,056**
N_6	0,030	**0,053**	0,028	0,047	0,028	0,047
C_7	0,021	0,043	0,027	**0,053**	0,027	**0,053**
C_8	**0,056**	0,027	**0,076**	0,038	**0,077**	0,038
C_9	0,016	**0,058**	0,049	**0,070**	**0,050**	**0,071**
C_{10}	**0,052**	**0,076**	**0,071**	**0,079**	**0,071**	**0,079**
N_{12}	0,009	0,046	0,016	0,045	0,016	0,045
Re_{13}	-0,008	0,009	-0,029	0,015	-0,029	0,016
C_{14}	0,023	0,012	0,045	0,017	0,046	0,017
O_{16}	**0,045**	**0,051**	0,031	0,039	0,031	0,039
O_{17}	**0,046**	0,044	0,031	0,035	0,031	0,035
C_{21}	0,029	-0,004	0,043	0,003	0,044	0,003
C_{37}	0,048	0,019	**0,051**	0,020	**0,052**	0,020
O_{38}	0,047	**0,058**	0,032	0,041	0,032	0,041
H_{40}	0,049	0,023	0,029	0,019	0,029	0,019
H_{41}	**0,051**	0,024	0,027	0,020	0,026	0,020
H_{42}	0,042	0,018	0,028	0,018	0,028	0,018
H_{43}	0,043	0,018	0,028	0,017	0,028	0,017
H_{44}	**0,050**	0,024	0,025	0,019	0,025	0,019
H_{45}	0,049	0,023	0,025	0,019	0,025	0,019
H_{46}	0,042	0,017	0,031	0,016	0,031	0,016
C_{56}	0,042	0,026	0,037	0,029	0,037	0,029

Acknowledgements

Scientific Research Projects Coordination Department of Ordu University (ODUBAP) under Grant Number AR-1657 supported this work.

References

[1] Hartinger CG, Dyson PJ. Bioorganometallic chemistry--from teaching paradigms to medicinal applications. *Chem Soc Rev* 2009; 38:391–401.
[2] Bitterwolf TE. Organometallic photochemistry at the end of its first century. J Organomet Chem.2004;689:3939–3952.
[3] Xu K, Peng H, Lam JWY, Poon TWH, Dong Y, Xu H, Sun Q, Cheuk KKL, Salhi F, Lee PPS, Tang BZ. Transition metal carbonyl catalysts for polymerizations of substituted acetylenes. Macromolecules 2000;33: 6918–6924.
[4] Üstün E, Ayvaz MÇ, Çelebi MS, Aşcı G, Demir S, Özdemir İ. Structure, CO-releasing property, electrochemistry, DFT calculation, and antioxidant activity of benzimidazole derivative substituted [Mn(CO)3(bpy)L]PF6 type novel manganese complexes. Inorganica Chim. Acta 2016;450:182-189.
[5] Vessieres A, Salmain M, Brossier P, Jaouen G. Carbonyl metallo immuno assay : a new application for Fourier transform infrared spectroscopy. J Pharm Biomed Anal 1999;21:625–633.
[6] Hostachy S, Policar C, Delsuc N. Re(I) carbonyl complexes: Multimodal platforms for inorganic chemical biology. Coordination Chemistry Reviews 2017;351:172–188.
[7] Johnson TR, Mann BE, Clark JE, Foresti R, Green CJ, Motterlini R. Metal carbonyls: A new class of pharmaceuticals? Angew. Chemie - Int. Ed. 2003;42:3722–3729.
[8] Mann BE, Motterlini R. CO and NO in medicine. Chem. Commun., 2007: 4197–4208.
[9] Hewison L, Crook SH, Johnson TR, Mann BE, Adams H, Plant SE, Sawle P, Motterlini R. Iron indenyl carbonyl compounds: CO-releasing molecules. Dalton Trans. 2010;39:8967–8975.
[10] Wysokiński R, Hernik K, Szostak R, Michalska D. Electronic structure and vibrational spectra of cis-diammine(orotato)platinum(II), a potential cisplatin analogue: DFT and experimental study. Chem. Phys. 2007;333:37–48.
[11] Rosa A, Ricciardi G, Baerends EJ, Stufkens DJ. Metal-to-ligand charge transfer (MLCT) photochemistry of fac-Mn(Cl)(CO)3(H-DAB): A density functional study J. Phys. Chem. 1996;100:15346–15357.
[12] Vummaleti SVC, Branduardi D, Masetti M, Vivo MD, Motterlini R, Cavalli A. Theoretical insights into the mechanism of carbon monoxide (CO) release from CO-releasing molecules. Chemistry 2012;18:9267–9275.
[13] Roy RK, Krishnamurti S, Geerlings P, Pal S. Local softness and hardness based reactivity descriptors for predicting intra- and intermolecular reactivity sequences: Carbonyl compounds. J. Phys. Chem. A 1998;102:3746–3755.
[14] Hazarika KK, Baruah NC, Deka RC. Molecular structure and reactivity of antituberculosis drug molecules isoniazid, pyrazinamide, and 2-methylheptylisonicotinate: A density functional approach. Struct. Chem. 2009;20:1079–1085.
[15] Neese F. Prediction of molecular properties and molecular spectroscopy with density functional theory: From fundamental theory to exchange-coupling. Coord. Chem. Rev. 2009;253:526–563.
[16] Neese F. The ORCA program system. Wiley Interdiscip. Rev. Comput. Mol. Sci. 2012;2:73–78.
[17] Neese F. A critical evaluation of DFT, including time-dependent DFT, applied to bioinorganic chemistry J. Biol. Inorg. Chem. 2006;11:702–711.
[18] Weigend F, Ahlrichs R. Balanced basis sets of split valence, triple zeta valence and quadruple zeta valence quality for H to Rn: Design and assessment of accuracy. Phys. Chem. Chem. Phys. 2005;7:3297.

IN SITU SYNTHESIS OF TRIGLYCERIDE OIL BASED POLYMER CLAY NANOCOMPOSITE

A. Tuncer ERCIYES[1], Yagmur BAYRAM[2], Emel AKYOL[2]

[1]Department of Chemical Engineering, Istanbul Technical University, Istanbul, Turkey.
erciyes@itu.edu.tr
[2]Department of Chemical Engineering, Yildiz Technical University, Istanbul, Turkey.
eakyol@yildiz.edu.tr

Abstract
In this study, oil based polymer-clay nanocomposites (OBPCNs) were synthesized by in-situ polymerization of oil based vinyl macromonomer with styrene in the presence of clay. The macromonomer was obtained by combining 2-hydroxyethyl methacrylate (HEMA) with partial glycerides. Then, the obtained macromonomer was copolymerized with styrene in the presence of organically modified clay. For the modification of clay, hexadecyltrimethylammonium (HDTMA) was used. Various amounts of clay were studied to determine the effect of clay content on nanocomposite properties. The structure of the oil based polymer clay nanocomposites were characterized by Fourier transform infrared spectroscopy (FTIR). Thermal gravimetric analysis (TGA) and differential scanning calorimetry (DSC) analysis were also applied for determination of the thermal characteristics. It was understood that triglyceride oil could be used for the preparation of nanocomposite product.
Key Words: *Oil based polymer-clay nanocomposites; in-situ polymerization; renewable source.*

1. Introduction

Polymer-clay nanocomposites have been attracted a great deal of attention due to their excellent properties such as high dimensional stability, thermal resistance, gas barrier performance, optical clarity, flame retardancy, and enhanced mechanical properties [1-4]. Kind of clay, composite preparation method, surface modification, dispersion of the clay in the polymer matrix has a great effect on the composite properties [3-5]. Dispersion of particles in polymeric matrixes has proved to be an effective and low-cost method to improve the performance of the nanomaterial properties such as mechanical properties, elasticity, transparency or specific absorption of light, optical properties, electrical conductivity, and, antimicrobial effects [6–11]. Triglyceride oils have been widely used in the preparation of polymers due to their environmental and energytical issues, and also for improving the end-product properties[12]. In this study, synthesis of oil based polymer-clay nanocomposites was achieved by using in-situ polymerization. It was understood that triglyceride oil could be used for the preparation of nanocomposite product.

2. Experimental

For the polymer matrix of composite system, oil based vinyl macromonomer were prepared by two successive steps. First, partial glycerides were obtained by glycerolysis reaction, and in the second step partial glycerides were combined with HEMA through urethane linkage by using toluene diisocyanate (TDI). Oil based macromonomer thus obtained was copolymerized with styrene in the presence of organically modified clay to achieve composite sample.. Copolymerization was started with free radicals stemming from the thermolysis of 2,2'-azoisobutyronitrile (AIBN). The obtained polymer nanocomposite structures were confirmed by FTIR (Perkin Elmer FT-IR Spectrum One B spectrometer) analysis. ture and thermal characteristics of the obtained composite samples were determined and the results were evaluated. Then samples were placed on a thin copper grid covered by a carbon film that supports the sample to be viewed. The thermal stability of the OBPCNs was measured using a TGA instrument (TA Instrument, TGA 2050) under a nitrogen atmosphere at a heating rate of 50˚C/min. For the determination of Tg values of samples differential scanning calorimetry (DSC Q200, TA Instruments) measurements were carried out under a nitrogen atmosphere at a heating rate of 20˚C/min.

3. Results and Discussions

As stated previously, triglyceride oil-based vinyl macromonomer was prepared in two successive steps. First, partial glycerides were obtained by glycerolysis reaction as depicted in Scheme 1. The hydroxyl and acid values (acid value, number of mg of potassium hydroxide to neutralize the acids present in 1 g of sample) of the partial glyceride were found to be 113 and 2.45, respectively.

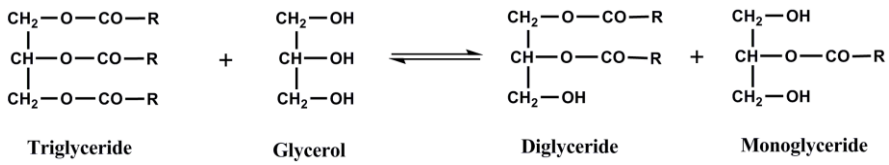

Scheme 1. Synthesis of partial glycerides.

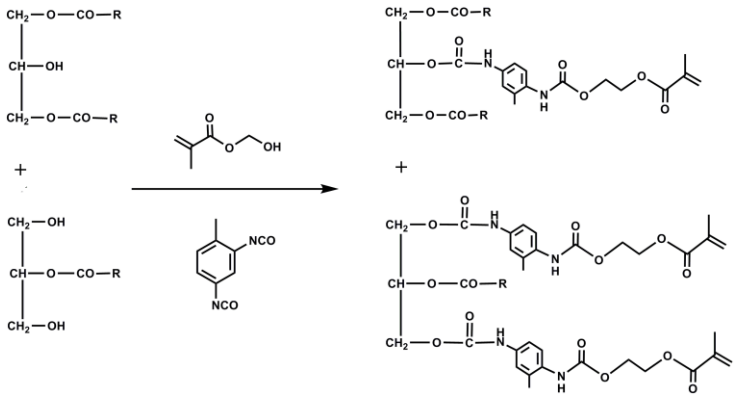

Scheme 2. Synthesis of macromonomer from partial glycerides.

Subsequently,, these partial glycerides were combined with HEMA through urethane linkage by using TDI (Scheme 2) in equivalent amount to total hydroxyl groups. The reaction between isocyanates and hydroxyl groups forming urethane linkage was monitored by FT-IR. In Figure 1, FT-IR spectra of initial reaction mixture containning partial glyceride, TDI and HEMA and the end product obtained after 4 h were given. As seen, the free isocyanate peak at 2270 cm^{-1} disappeared after 4 h indicating completion of the reaction. As illustrated in Scheme 2, polymerizable methacrylate double bonds were inserted into the structure through the hydroxyl groups of mono- and diglycerides. The unsaturated terminal groups are expected also to act as cross-linker in the subsequent polymerization step. The number average molecular weight of the macromonomer was determined by GPC and found to be 3280 with a polydispersity of 2.21. The observed relatively high polydispersity is expected since the partial glycerides used to obtain macromonomer is a mixture of mono, di and triglycerides. Styrene monomer was copolymerized with the macromonomer by using AIBN as free radical initiator in the presence of OCLAY. The radicals stemming from the thermal decomposition of AIBN initiate the polymerization.

FTIR analysis was also applied to the organomodified clay (OCLAY). The obtained spectra were given in Figure 1 for OCLAY. As seen in Figure 1, the bands related to OCLAY were found, such as OH stretching of lattice water (3622 cm^{-1}), H–O–H bending (1642 cm^{-1}), Si–O–Si stretching (1045 cm^{-1}). TGA analysis of oil based polymer and its nanocomposites with different clay loadings are shown in Figure 2. These results showed that, regarding thermal stability polymer-clay nanocomposite samples were poorer compared to pure polymer. $T_{10\ wt.\ \%}$(°C) values showed that the increase of clay amount caused the sample to have low thermal stability. Similar results were also observed by Xinfeng et al [13]. This result is most probably due to the catalytic effect of clay due to its water and hydroxyl groups. As expected, the char yield was increased with increasing the clay loading. DSC analysis and the obtained results were given in Figure 3 and Table 1. The glass transition temperature (T_g) of the cured OBP was found to be higher than that of OBPNC samples. The values of T_g decreased from 133.67 to 116.71°C with increasing clay loading from 0.75 to 3 wt%. This kind of behaviour was also observed by Lakshmi et al [14]. They investigated epoxy-clay nanocomposites and found that up to 5% clay loading Tg decreased. The reason of this decrease was explained as the preventing of 3D network formation in the presence of clay. Additionally, Nagendiran et al. [15] were studied organic-inorganic hybrids involving cyanate ester and HTPDMS (hydroxyl terminated polydimethylsiloxane) modified epoxy, filled with organo-modified montmorillonite clay. For the decrease in Tg with increasing clay loading, they gave the same explanation as the one mentioned above. However, for the decrease of Tg they additionally pointed out that the plasticization effect imparted by surface modifier (cetylammonium ion) within the organoclay. At the end of this study the obtained preliminary results showed that oil modified polymer could be used for the preparation of nanocomposite materials.

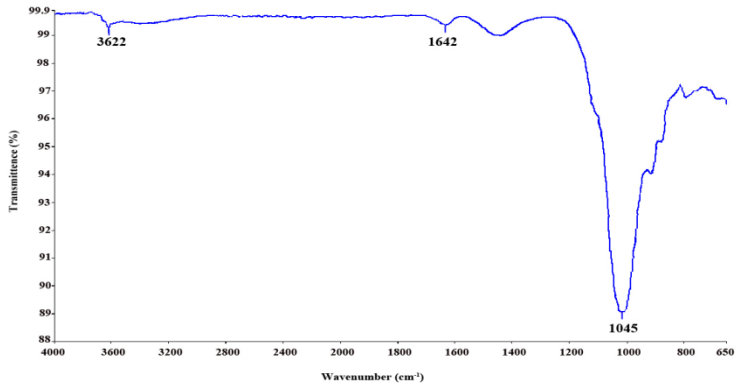

Fig.1. FTIR spectra of OCLAY

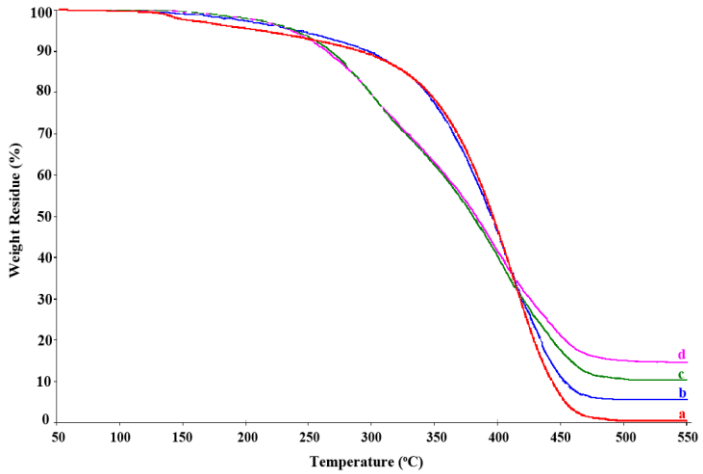

Fig. 2. TGA curves of (a) pure OBP and its nanocomposites containing (b) 0.75, (c) 1.5 and (d) 3 wt% of clay.

Table 1. Cp and Tg values of OBP and its nanocomposites (OBPCN) with different clay loadings.

Sample	Clay %	Cp (J/g ˚C)	Tg (˚C)
OBP	-	1.448	135.56
OBPCN	0.75	0.102	133.67
OBPCN	1.5	1.204	129.17
OBPCN	3	1.813	116.71

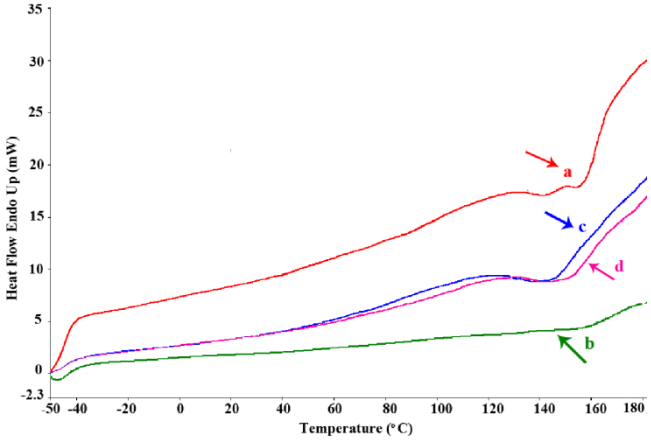

Fig. 3. DSC curves of (a) OBP and OBPCNs nanocomposites containing (b) 0.75, (c) 1.5 and (d) 3 wt% of clay

4. Conclusion

In this study oil based polymer was used in the preparation of polymer-clay nanocomposites. Sunflower and MMT were used for the oil and clay components. In the synthesis of oil based polymer, a strategy based on macromonomer technique was applied. Macromonomer was obtained by combining the partial glyceride with HEMA through the reaction with TDI. The macromonomer thus obtained was copolymerized with styrene in the presence of clay. The resulting product is a polymer-clay nanocomposite material. The preliminary results obtain in study showed that oil based polymer could be used for the production of nanocomposite materials. The point which should be emphasized that the use of triglyceride oil is considered to be the important class of renewable source in nanocomposite preparation. It is well known that recently the use of renewable sources in the industrial product has gained more importance due to environmental concerns and additionally diminishing of the natural sources.

References

[1] Okamoto M. Recent advances in polymer/layered silicate nanocomposites: an overview from science to technology. Mater Sci Technol 2006; 22:756-779.

[2] Ray SS, Okamoto M . Polymer/Layered Silicate Nanocomposites: A Review Form Preparation to Processing. Prog Polym Sci 2003;28:1539-1641.

[3] Pettarin V, Frontini PM, Pita VJR, Dias ML, Diaz FV. Polyethlene/(organo-montmorilloite) composite modified with ethylene/methacrylic acid copolymert: Morphology and mechanical properties. Composites: Part A 2008;39:1822-1828.

[4] Demirkol EA, Kalyon DM. Batch and continuous processing of polymer layered organoclay nanocomposites. J Appl Polym Sci 2007;104:1391-1398.

[5] Zhu L, Wool RP. Nanoclay reinforced bio-based elastomers: synthesis and characterization. Polymer 2006;47:8106-8115.

[6] Forster S, Antonietti M. Amphiphilic Block Copolymers in Structure -Controlled Nanomaterial Hybrids. Adv Mater 1998;10:195-217.

[7] Mayer, ABR. Colloidal metal nanoparticles dispersed in amphiphilic polymers. Polym Adv Technol 2001;12, 96-106.

[8] Beecroft LL. Ober CK. Nanocomposite Materials for Optical Applications. Chem. Mater 1997;9:1302-1317.

[9] Caseri, W. Nanocomposites of polymers and metals or semiconductors: Historical background and optical properties. Macromol Rapid Commun 2000;21:705-722.

[10] Gangopadhyay R. De A. Conducting Polymer Nanocomposites: A Brief Overview. Chem Mater 2000;12:608-622.

[11] Kane RS. Cohen RE. Silbe, R. Synthesis of PbS Nanoclusters within Block Copolymer Nanoreactors. Chem Mater 1996;8:1919-1924.

[12] Eksik O. Erciyes AT. Yagcı Y. J. In situSynthesis of Oil Based Polymer Composites ContainingSilver Nanoparticles. Macromol. Sci 2008;45:698-704.

[13] Xinfeng X. Yanfen D. Feng W. Bin W. Junhua Z. Shimin Z. Mingshu Y. Effects of Silane Grafting on the Morphology and Thermal Stability of Poly(ethylene terephthalate)/Clay Nanocomposites. Polym Compos 2010;31:825-834.

[14] Lakshmi MS. Narmadha B. Reddy BSR. Enhanced thermal stability and structural characteristics of different MMT-Clay/epoxy-nanocomposite materials. Polym Degrad Stabil 2008;93:201-213.

[15] Nagendiran S. Chozhan CK.. Alagar MK. Hamerton I. Inorganic/organic hybrid nanocomposites involving OMMT clay and cyanate ester-siloxane-modified epoxy resin: Thermal, dielectric and morphological properties. High Perform Polym 2008;20: 323-347.

PREPARATION OF A NOVEL GOLD NANOCLUSTER-BASED BIOSENSOR USING EGG WHITE PROTEIN AND ITS APPLICATION FOR MEASURING PROOXIDANT ACTIVITY

Esin AKYÜZ[1], Furkan Burak ŞEN[1], Mustafa BENER[1], Kevser SÖZGEN BAŞKAN[1], Esma TÜTEM[1], Reşat APAK[1,2]

[1]Department of Chemistry, Faculty of Engineering, Istanbul University-Cerrahpasa, Avcilar, 34320 Istanbul, Turkey

[1,2]Turkish Academy of Sciences (TUBA), Piyade St. No: 27, Çankaya, Ankara 06690, Turkey

Abstract

In this work, chicken egg white protein (CEW)-protected gold nanoclusters (CEW-AuNCs) were prepared to measure the Cu(II)-induced prooxidant activity of antioxidant compounds such as epicatechin, epigallocatechin gallate, catechin, rosmarinic acid, resveratrol, ascorbic acid, and glutathione. This assay involved the reduction of Cu(II) ions to Cu(I) by antioxidant compounds (simultaneously giving rise to reactive oxygen species) and binding of the formed Cu(I) to the CEW-AuNC structure. The bound Cu(I) may be released with the cuprous-selective ligand neocuproine (Nc), forming the basis of a spectrophotometric method measuring absorbance at 450 nm pertaining to the Cu(I)−Nc chelate. The order of the molar absorption coefficients of the tested compounds with respect to the CEW-AuNC biosensor were: epigallocatechin gallate > epicatechin > catechin > resveratrol > glutathione > ascorbic acid ≥ rosmarinic acid. The developed method involved a one-pot synthesis and determination without tedious separations, and was applied to binary synthetic mixtures of studied antioxidant compounds and to certain herbal plant (green tea, linden, echinacea, and artichoke leaf) extracts to determine the total prooxidant activities. The results were statistically compared with those of a literature Cu(II)−Nc assay using a calcium proteinate-based solid biosensor. The developed biosensor was stable, reliable, easily applicable, of low cost and wide linear range, and could reproducibly determine the prooxidant activities of natural antioxidant samples.

Key Words: *Chicken egg white proteins (CEW); gold nanocluster (AuNC); CEW-AuNC prooxidant biosensor; cuprous-neocuproine; natural antioxidants*

1. Introduction

Oxidative stress occurs when antioxidants and oxidants/prooxidants are not balanced in favour of the latter, which may cause biomacromolecular damage leading to various diseases [1]. Although the main health beneficial effects of natural bioactive compounds originate from their antioxidant properties, they may exhibit prooxidant behavior under certain conditions (such as transition metal ions and O_2) [2]. The prooxidant activity is the ability of reducing transition metal ions to their lower oxidation states by antioxidant compounds, stimulating the production of reactive species which can cause various diseases via Fenton-type reactions [3]. Therefore, understanding the antioxidant/prooxidant behavior of bioactive substances depending on structures and conditions in which they are found is of great importance.

Gold nanoclusters (AuNCs) may be distinguished for their facile synthesis, good solubility and fluorescence, photostability, biocompatibility, and reduced toxicity [4]. As opposed to many toxic and environmentally unfriendly organic substances frequently used as reducing or protection agents for the synthesis of noble metal nanoparticles, various biological molecules have recently been used in fluorescent NP/NC synthesis, aiming to overcome biocompatibility related problems [5].

In this study [6], chicken egg white protein-protected gold nanoclusters (CEW-AuNCs) were prepared to measure the transition metal ion {Cu(II)}-catalyzed prooxidant activities of antioxidant compounds, and accordingly, a spectrophotometric method was developed utilizing Cu(II)→Cu(I) reduction by antioxidants, uptake of Cu(I) by CEW-AuNC, followed by desorption of Cu(I) from the sensor matrix with the aid of neocuproine (Nc) to produce the chromophore: Cu(I)-Nc chelate having yellow-orange color and strong absorbance at 450 nm. The developed method was applied to binary synthetic mixtures of studied compounds and to herbal plant extracts for determining total prooxidant activities. The obtained results were statistically compared with those of the Cu(II)-Nc assay using calcium proteinate solid biosensor [7].

2. Materials & Methods

The egg white was separated from yolk; lyophilized by freeze-dryer until completely dry, and then was powdered by grinding in a mortar. The protein solution (at 10 mg mL^{-1}) was prepared by dissolving this powder in distilled water.

The CEW-AuNCs were synthesized after slight modification of the method of Li et al. (2017) [8]. Briefly, 25 mL of 10 mg mL^{-1} protein solution was added to 25 mL 2.5 mM $HAuCl_4$ solution which was diluted from the stock solution at 1.49 M, and vortexed for 2 min. To the mixture, 3.5 mL of 1 M NaOH solution was added and incubated in a 37 °C water bath for 20 hours. After the incubation period, the formed CEW-AuNCs were stored in the refrigerator at 4 °C before use.

The contents of the binary mixtures were given below:

Mixture 1: 30.7 µM ECAT + 307.7 µM AA
Mixture 2: 307.7 µM AA + 307.7 µM RA
Mixture 3: 61.5 µM RES + 615.4 µM GSH

2.1. Cu(II)-Nc assay using CEW-AuNC–based biosensor

The mixture of CEW-AuNC, phosphate buffer (pH 7.4), Cu(II) and antioxidant solutions was incubated at room temperature for 30 min. Afterwards, EDTA solution was added to eliminate excessive Cu(II) in the medium and vortexed. To the mixture, Nc was added to obtain Cu(I)-Nc complex and the absorbance at 450 nm was measured against blank solution.

2.2. Cu(II)-Nc Assay using Calcium Proteinate-Based Solid Biosensor

This method [7], developed by our study group, was based on the measurement of the 450 nm-absorbance of Cu(I)-Nc chelate formed by neocuproine with protein bound copper(I) ion. Briefly, the solid prooxidant sensor was incubated with Cu(II) ion in a medium containing phosphate buffer and antioxidant solution at different concentrations. At the end of this period, the aqueous phase was decanted and the solid prooxidant sensor was washed with pure water to eliminate the interference effects that could come from unreacted compounds. During the second incubation step, the Cu(I)-Nc chelate was extracted with ethanolic neocuproine from solid protein to the solution phase, and absorbance was measured at 450 nm.

3. Results & Discussion

Since the proposed CEW-AuNC assay was performed in solution medium, EDTA was added to accurately quantify the protein bound-Cu(I) as an expression of prooxidant activity. The remaining excess Cu(II) ion in the medium is complexed with EDTA to prevent binding with Nc to be added. If the free Cu(II) remains in the medium, Cu(II)-Nc (formed after addition Nc) and antioxidant reaction is continued which is cause to positive error in the determination of prooxidant activity. As a result, the EDTA ligand plays a role in both the stopping to the antioxidant-Cu(II) reaction and the preventing to formation of the Cu(II)-Nc complex. In this respect, the interference effects that might arise from the solution medium were eliminated with adding EDTA.

Limit of detection (LOD) and limit of quantification (LOQ) as well as intra- and interday reproducibility (i.e., within- and between run precision) of the proposed method as analytical performance for the chosen standard compound (ECAT) were given in Table 1. Correlation coefficients (r) and linear ranges (µM) for the tested antioxidant compounds (ECAT, CAT, EGCG, AA, RA, RES, and GSH) with respect to the Cu(II)-Nc assays using both soluble CEW-AuNC and solid calcium proteinate-based biosensors were shown in Table 2. The order of the molar absorption coefficients of the tested compounds with respect to the CEW-AuNC and solid protein-based Cu(II)-Nc assays were: EGCG > ECAT > CAT > RES > GSH > AA ≥ RA, and EGCG > ECAT > CAT > GSH > AA, respectively. The molar absorption coefficients of antioxidants followed the same order for the two assays, except for the compounds which could not be detected with the reference method.

Table 1. Comparison of figures of merit of the biosensors based on soluble CEW-AuNC and solid protein tested on ECAT standard (n = 3).

Parameter	CEW-AuNC based Cu(II)-Nc assay	Solid protein based Cu(II)-Nc assay
Linear range (µM)	15.4 – 77	12.5 – 150
LOD (µM)	0.9	1.2
LOQ (µM)	3.0	4.0
Linear equation	A= 1809 c + 0.012	A= 3472 c + 0.142
Correlation coefficient (r)	0.9977	0.9907
Within-run precision	1.3	2.8
Between-run precision	3.4	3.2

Table 2. Linear regression equations, correlation coefficients (r), and dynamic linear concentration ranges of the tested compounds with respect to the Cu(II)-Nc assays applied on CEW-AuNC sensor and solid Ca-proteinate sensor (N = 3).

Tested compound	CEW-AuNC based Cu(II)-Nc assay		Solid protein-based Cu(II)-Nc assay	
	Linear regression equation, and correlation coefficient (r)	Linear range (µm)	Linear regression equation, and correlation coefficient (r)	Linear range (µm)
ECAT	A = 1809 c + 0.012 r = 0.9977	15.4 – 77.0	A = 3472 c + 0.142 r = 0.9907	12.5 – 150.0
CAT	A = 1424 c + 0.018 r = 0.9951	15.4 – 77.0	A = 2295 c + 0.201 r = 0.9996	25 – 250
EGCG	A = 3351 c + 0.019 r=0.9993	7.7 – 76.9	A= 16354 c – 0002 r= 0.9928	6.3 – 31.3
AA	A = 122 c + 0.006 r = 0.9921	154 – 615	A = 142 c + 0.068 r = 0.9998	250 – 2500
RA	A = 115 c + 0.035 r = 0.9974	308 – 1538	n.d.	n.d.
RES	A = 780 c + 0.041 r = 0.9983	61.5 – 307.7	n.d.	n.d.
GSH	A = 732 c - 0.115 r = 0.9945	308 – 1538	A = 1092 c - 0.010 r = 0.9875	50 – 125

n.d. not detected

Total prooxidant activities of prepared synthetic mixtures were found as mM ECAT equivalents by dividing the observed absorbance (A_{450}) to the molar absorptivity of ECAT, and compared with those theoretically found (Table 3). The experimental and theoretical TPA values of the synthetic mixtures were compatible with each other, where these capacities agreed at 95% confidence level ($F_{calculated}$ = 0.197, $F_{critical}$ = 18.513, $F_{calculated} < F_{critical}$ at p = 0.05).

Table 3. Experimental and theoretical TPA values of synthetic mixture solutions of tested compounds as mM ECAT equivalent (n = 3).

Sample	Cu(II)-Nc assay using CEW-AuNC	
	Experimental TPA	Theoretical TPA
Mixture 1	0.80 ± 0.01	0.73
Mixture 2	0.90 ± 0.02	0.96
Mixture 3	1.23 ± 0.01	1.30

Green tea (*Camellia sinensis*), linden (*Tilia*), echinacea (*Echinacea purpurea*), and artichoke leaf (*Cynara scolymus*) were studied as real samples. Evaluation of recovery values for the CEW-AuNC based biosensor were realized by spiking two different concentrations of ECAT solution at 0.1 and 0.2 mM to the diluted herbal extracts. Statistical data were given in terms of spiked, theoretical (Theo.) and experimental (Exp.) mM ECAT equivalents in Table 4. The obtained recovery values (Rec.) close to 100% indicated that the CEW-AuNC based biosensor was reliable to determine TPA values of plant extracts containing natural antioxidants.

Table 4. ECAT recoveries from herbal infusions using the CEW-AuNC based Cu(II)-Nc assay (n = 3).

Herbal plant	Added (mM)	Theo. (mM)	Exp. (mM)	Rec. (%)	R.S.D. (%)
1:10 dilluted echinacea	0.20	0.35	0.34±0.01	97	2.9
	0.40	0.55	0.56±0.01	102	1.8
1:10 diluted green tea	0.20	0.79	0.79±0.03	100	3.8
	0.40	0.99	1.05±0.01	106	0.9
1:5 diluted linden	0.10	0.52	0.52±0.02	100	3.8
	0.20	0.62	0.60±0.01	97	1.7
1:10 diluted artichoke leaf	0.20	0.34	0.35±0.02	103	5.7
	0.40	0.54	0.58±0.01	107	1.7

Acknowledgements

The authors thank Istanbul University-Cerrahpasa Application & Research Center for the Measurement of Food Antioxidants (IU-C GAAM) for sharing its research infrastructures. Authors also acknowledge Istanbul University Research Fund, Bilimsel Arastirma Projeleri (BAP) Yurutucu Sekreterligi, for the support given to their Project FBA-2018-28955.

References

[1] Lü JM, Lin PH, Yao Q, Chen C. Chemical and Molecular Mechanisms of Antioxidants: Experimental Approaches and Model Systems. *J. Cell. Mol. Med.* 2010;**14(4)**:840-860.

[2] Rietjens IMCM, Boersma MG, Haan L, Spenkeiink B, Awad HM, Cnubben NHP, Zanden JJ, Woude H, Alnk GM, Koeman JH. The Pro-Oxidant Chemistry of the Natural Antioxidants Vitamin C, Vitamin E, Carotenoids and Flavonoids. *Environ. Toxicol. Phar.* 2002;**11**:321-333.

[3] Zeraik ML, Petrônio MS, Coelho D, Regasini LO, Silva DHS, da Fonseca LM, Machado AS, Bolzani VS, Ximenes VF. Improvement of Pro-Oxidant Capacity of Protocatechuic Acid by Esterification. *Plos One*. 2014;**9**:1-9.

[4] Li Z, Peng H, Liu J, Tian Y, Yang W, Yao J, Shao Z, Chen X. Plant Protein-Directed Synthesis of Luminescent Gold Nanocluster Hybrids for Tumor Imaging. *ACS Appl. Mater. Inter.* 2018;**10**:83-90.

[5] Ding H, Yang D, Zhao C, Song Z, Liu P, Wang Y, Chen Z, Shen J. Protein−Gold Hybrid Nanocubes for Cell Imaging and Drug Delivery. *ACS Appl. Mater. Inter*. 2015;**7**:4713-4719.

[6] Akyüz E, Burak Şen F, Bener M, Sözgen Başkan K, Tütem E, Apak R. Protein-Protected Gold Nanocluster Based Biosensor for Determining Prooxidant Activity of Natural Antioxidant Compounds. *ACS Omega* 2019;**4**:2455-2462.

[7] Akyüz E, Sözgen Başkan K, Tütem E, Apak R. Novel Protein-Based Solid-Biosensor for Determining Pro-Oxidant Activity of Phenolic Compounds. *J. Agr. Food Chem.* 2017;**65**:5821-5830.
[8] Li XJ, Ling J, Han CL, Chen LQ, Cao QE, Ding ZT. Chicken Egg White-Stabilized Au Nanoclusters for Selective and Sensitive Detection of Hg(II). *Anal. Sci.* 2017;**33(6)**:671-675.

Steric and Electronic Requirements for Atropisomerization in Heterocyclic Analogues of Biaryls

İlknur DOĞAN

Boğaziçi University Department of Chemistry 34342 Bebek İstanbul Turkey dogan@boun.edu.tr

Abstract

Atropisomers are enantiomers or diastereoisomers that result from slow axial rotation that can, in principle, interconvert thermally, but for which the half-life of interconversion is ~1000 s or longer, thus allowing analytical separation [1]. The slow rotation along a bond axis usually results from steric hindrance and/or electronic factors. This work describes the steric and electronic requirements needed to produce stable heterocyclic nonbiaryl atropisomers with an Nsp2-Caryl stereogenic axis and the reasons for the observation of high barriers to rotation are discussed. Rotational barriers caused by the effects of the same substituents on different frameworks have been compared and they have been found to correlate very well with each other.

Key Words: Atropisomers; Axial chirality; Nonbiaryl axially chiral compounds; Temperatur dependent NMR; Thermal racemization

1. Introduction

Axially chiral enantiomers result from slow axial rotation around a chiral axis and they are thermally interconvertible. The most commonly encountered axially chiral compounds occur among biphenyl derivatives, where the groups R_1, R_2 and R_3, R_4 (figure 1) are too large to pass each other freely causing an intramolecular hindered rotation. As a result of this the ground states of the molecules become non-planar and thus enantiomeric. Heterocyclic analogues of biphenyl systems comprise compounds where a heterocyclic ring is perpendicular (or nearly so) to the *ortho*-substituted phenyl ring. Here, the exocyclic substituents of the heterocyclic ring and the *ortho*-substituent on the phenyl ring cannot pass each other freely, resulting in a dihedral between the two rings. If the half-life of interconversion between the axially chiral enantiomers is~1000 s or longer at a given temperature, the **M** and **P** forms are called as atropisomers. Since they are stable at ambient temperature analytical and preparative separation of them become feasible. If there is another chiral element in the molecule such as a chiral center, the rotation this time will convert the diastereomers to each other.Barrier to hindered rotation is the energy difference between the ground state and the transition state conformations of the axially chiral molecules (figure 2). The ground state is nonplanar and the transition stete state is planar and the difference in energy between them is the activation energy for rotation. Steric hindrance and/or electronic factors account for the slow rate of interconversion, leading to atropisomerism. To be able to predict the barriers to rotation will be useful in designing and planning the synthesis of atropisomeric systems. Roussel *et al* recently developed a steric scale for some common substituents that can be used for such predictions [2].

2. Results and Discussion

The barriers to rotation have been determined by either temperature dependent ^{1}H NMR [3] or by thermal racemization of the micropreparatively resolved atropisomers [4,5]. The barriers caused by the same substituents on different frameworks were compared with each other and an excellent correlation has been found in each case.

The energy barriers of the halogen series of the axially chiral heterocyclics were found to increase linearly with the van der Waals radius of the *ortho* substituded halogen atom. On the other hand, although the van der Waals radius of the methyl group is larger than that of the chlorine atom, the chlorine atom was found to cause a larger steric effect than the methyl group in all of the frameworks studied and this was attributed to the electronic effect caused by the chlorine atom. The lone pairs of electrons of the chlorine apparently interacts with the lone pairs of electrons of the exocyclic oxygen atom of the heterocyclic rings causing a larger barrier. The activation energies for rotation (rotational barriers) caused by the the same substituents on different frameworks were found to show an excellent correlation (figures 3 and 4).

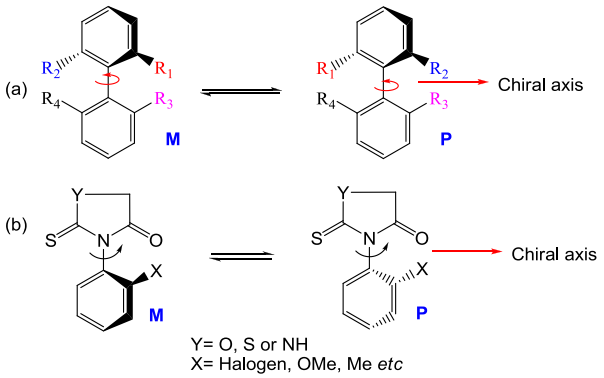

Fig. 1. (a) Axially chiral biphenyls; (b) axially chiral nonbiaryl heterocylic compounds (Times New Roman, 8pt)

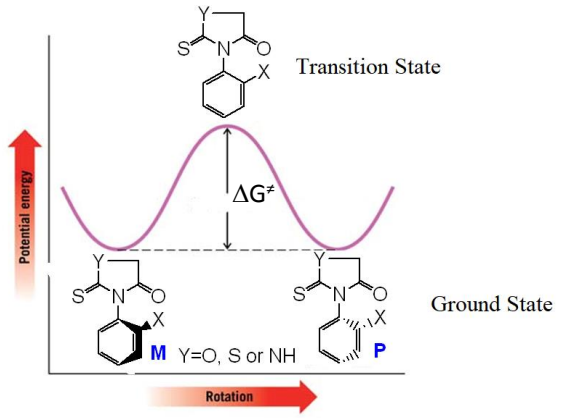

Fig. 2. Activation energy (Rotational barrier, $\Delta G^{\neq}$) for interconversion between the enantiomers in axially chiral compounds.

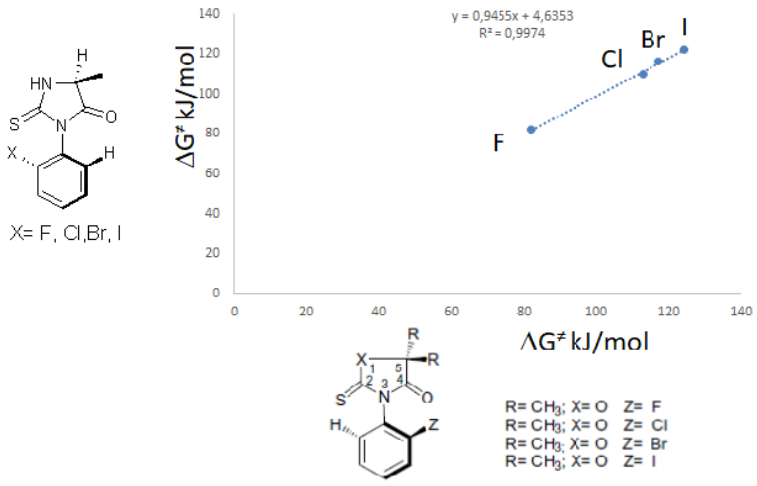

Fig. 3. Comparison of the activation barriers determined for halogenated thiohydantoins [4] with halogenated oxazolidinthions [5].

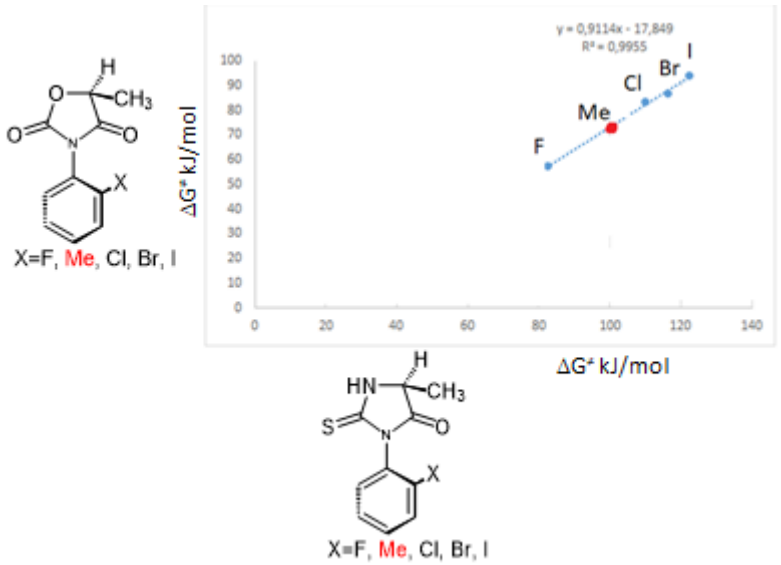

Fig. 4 Comparison of the activation barriers determined for oxazolidindione derivatives[3] with thiohydantoin derivatives [4].

3. Conclusion

Because the rotational barriers caused by the effects of the same substituents on different frameworks showed an excellent correlation, knowing the energy barriers for a few substituents for a given framework will enable to predict the energy of activation that will be caused for some other substituents.

References

[1] LaPlante SR, Edwards PJ, Fader LD, Jakalian A, Hucke O. Revealing Atropisomer Axial Chirality in Drug Discovery. ChemMedChem.2011;6:505–513.

[2] Belot V, Farran D, Jean M, Albalat M, Vanthuyne N, Roussel C. Steric Scale of Common Substituents from Rotational Barriers of N-(o-Substituted aryl)thiazoline-2-thione Atropisomers. . J. Org. Chem. 2017;82: 10188-10200.

[3]] Demir Ö, Doğan İ. Conformational Preferences in Diastereomeric (5S)-Methyl-3-(o-aryl)-2,4-oxazolidinediones. Chirality. 2003;15:242-250.

[4] Sarigul S. and Dogan I. Atroposelective Synthesis of Axially Chiral Thiohydantoin Derivatives. J. Org. Chem. 2016.;81:5895−5902 [5] Fachinger, J., 2006. Behavior of HTR Fuel Elements in Aquatic Phases of Repository Host Rock Formations. Nuclear Engineering & Design 236, p. 54.

[5] Yılmaz EM and Dogan I . Axially chiral N-(o-aryl)-2-thioxo-oxazolidine-4-one and rhodanine derivatives: Enantiomeric separation fuel determination of racemizatıon. Tetrahedron:Asymmetry. 2008;19:2184-2191.